Agency to which Report is Submitted:	DOE/EERE Solar Technologies office	
FOA Name:	Transformational PV Science and Technology	
FOA Number:	DE-FOA-0000387	
Report:	Final Technical Report	
Award Type:	Cooperative Agreement	
Award Number:	DE-EE0005315	
Prime Recipient:	Princeton University	
Prime Recipient Type:	University	
Project Title:	HOLE-BLOCKING LAYERS FOR SILICON/ORGANIC HETEROJUNCTIONS: A NEW CLASS OF HIGH-EFFICIENCY LOW-COST PV	
Principal Investigator (PI):	James Sturm, Professor, sturm@princeton.edu; 609-258-5610	
DOE Technology Manager (TM):	Dana Olson	
DOE Technical Project Officer (TPO):	Christopher Anderson	
DOE Grants Management Specialist (GMS):	Denise Moody	
DOE Contracting Officer (CO):	Andrew J. Ritters	
Prime Recipient DUNS Number:	00-248-4665	
Award Period of Performance (POP):	Start: 09/01/2011	End: 08/31/2016
Award Budget Period (BP):	Start: 09/01/2011	End: 08/31/2016
Date of Report:	12/04/2017	
Reporting Period (covered by this report):	09/01/2011 to 08/31/2016	

Table of Contents

Abstract

This project is the first investigation of the use of thin titanium dioxide layers on silicon as a hole-blocking / electron-transparent selective contact to silicon. The work was motivated by the goal of a high-efficiency low-cost silicon-based solar cells that could be processed entirely at low temperature (300 ^{o}C) or less, without requiring plasma-processing.

The work in this project:

- Demonstrates a new way to grow TiO_2 with a single precursor at the lowest temperature yet reported for a chemical vapor deposition process (100 ^{o}C) (Task 1)
- Measures the basic interface properties and band offsets of Si/TiO_2 (Task 2)
- Measures a very low and stable interface recombination at Si/TiO_2 (Task 3)
- Integrates the material into a silicon photovoltaic device with 100 ^{o}C maximum process temperature (Task 4).

The results show that the Si/TiO_2 selective contact, with current interface recombination properties, can replace the conventional n/n^+ back-side field structure, and support a power efficiency 21- 23%.

I. Introduction

I.A. Carrier-selective contacts to replace p-n junctions

Crystalline (and to a lesser extent polycrystalline) solar cells offer relatively high efficiency due to long minority carrier lifetimes and the ability to easily separate nearly all generated electron-hole pairs, leading to a near-ideal photocurrent. On the other hand, the need for at least one high-temperature (> 800 °C) diffusion for the p-n junction, and possibly a second for highest efficiency (to create the back-side field at the substrate contact for a high open-circuit voltage) can add to cost. The goal of this project is to investigate the fundamental materials and application issues related to replacing one of those p-n junctions with a hole-blocking (and electron-transparent) heterojunction on top of the silicon surface using a low-cost low-temperature technology.

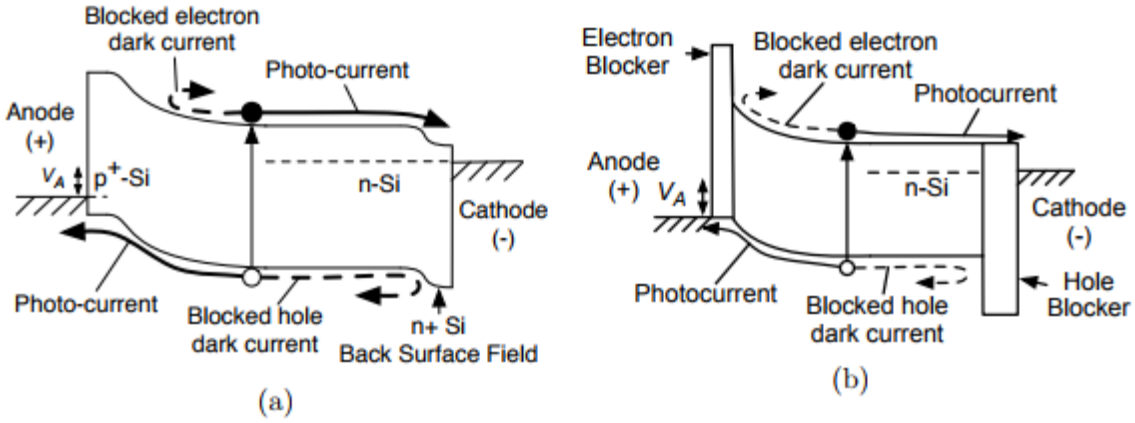

Figure 1. Comparison of (a) conventional n-type silicon solar cell with (b) ideal heterojunction solar cell under illumination and forward bias. The p^+ emitter and n^+ BSF are replaced with electron-blocking (and hole-transparent) and hole-blocking (and electron-transparent) heterojunctions, respectively.

Figure 1(a) show the band diagram of a conventional high-efficiency silicon solar cell. The left side is the p-n junction, which creates the field to separate electrons and holes. In forward bias, this junction has the (unwanted effect) of injecting minority carrier holds into the substrate. Even with infinite bulk lifetime, they will recombine at the back contact, setting up a hole

concentration gradient from left to right in the substrate. Diffusion driven by the gradient leads to dark current, which degrades the open-circuit voltage. Thus, heavy n-type doping is often used at the contact – it sets up a retarding field to somewhat (not completely) reduce the hole current from left to right. The main goal of this project is to replace the n^+ back side diffusion step with the deposition of a semiconductor which has a conduction band that approximately matches that of silicon so electrons (as photocurrent) can go through, but with a valence band edge much below of that of silicon to block the holes – a "hole-blocker" (Figure 1(b).) To be technologically attractive, this deposition process should occur under ~300 ^oC).

Also shown in in Figure 1(b) is the substitution of an "electron-blocking" (hole-transparent) heterojunction to replace the p-n junction. The high conduction band stops electrons from moving towards the left contact (the anode) under forward bias, similar to the built-in barrier of a p-n junction. The layer must have minimal valence band offset compared to silicon, as photocurrent (e.g. holes) moves from the silicon to the anode. In our previous work we have showed that polythiophene (P3HT) or PEDOT:PSS thin (~10 nm) organic layers can fulfill this role [S. Avasthi, S. Lee, Y. L. Loo, and J. C. Sturm, "Role of majority and minority carrier barriers silicon/organic hybrid heterojunction solar cells," Advanced Materials, vol. 23, pp. 5762-+ (2011). doi: 10.1002/adma.201102712]. Using a high-work-function metal and/or high-work-function doped PEDOT, a built-in field near the silicon surface results, which separates electrons and holes to give photocurrent. These layers are deposited typically (and in our work) by spin coating, so they can indeed be deposited by "low-temperature" and potentially "low-cost" processes. Finally, we note that with minimal valence band offset, holes can be injected from the anode into the n-type substrate.

A cell architecture like that in Figure 1(b) is also attractive because it has no heavy doping at either the anode or cathode contact. Heavy doping can lead to band-gap narrowing, which can reduce open-circuit voltage, and to Auger recombination, which can reduce photocurrent (and indirectly reduce open-circuit voltage as well).

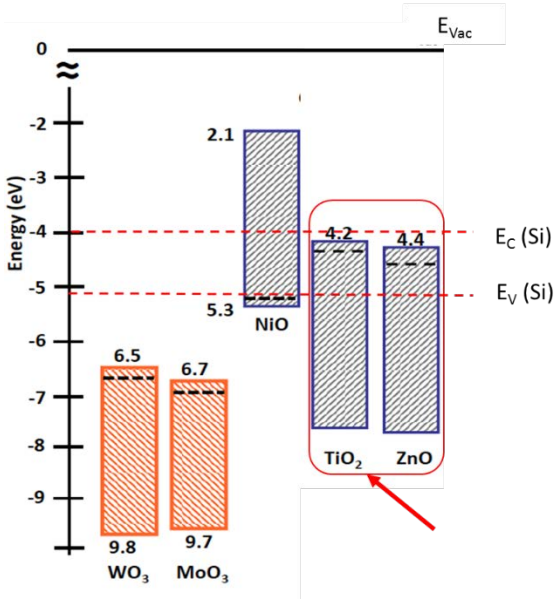

Figure 2. Calculated conduction band and valence band edges (indicated by shaded bandgap) for various metal oxide semiconductors. Also shown for reference are the conduction band and valence band edge of silicon compared to the vacuum level. TiO_2 seems the best candidate for use as a hole-blocker while allowing electrons to pass in either direction [from Ratcliff et al., J. Phys. Chem. Lett. (2011)].

This project originally sought to implement the hole-blocking layer using organic materials. However, the emergence of metal oxide semiconductors in widespread application led us to examine this class of materials. For example, InGaZnO (IGZO) thin film transistors are now used in every pixel of many flat panel displays on glass to control pixel addressing. Shown in Figure 2 are the calculated conduction and valence band edges for several metal oxide semiconductors, along with the conduction and valence band edges of silicon. ZnO and especially

TiO_2 seem especially good targets for a hole-blocking layer because their E_V is well below that of Si. For electron transparency, needed to let photocurrent of electrons through the layer to the cathode, TiO_2 seems the better choice, because of its better match in conduction band to silicon. Thus we chose titanium dioxide as the target material for a hole-blocking /electron-transparent contact to silicon as the focus of this project. TiO_2 is also widely used in organic solar cells as an electron blocker.

I.B. Effect of Interface States and Interface Recombination

Because holes are minority carriers in the n-type silicon (as in Figure 1(b)), the blocking contact should not cause their recombination. Thus the midgap defects at the Si/ TiO_2 interface are of great interest (Figure 3). They lead to a hole recombination, which is typically characterized by a surface recombination velocity. The interface recombination rate (R_{int}) is given by:

$$R_{\text{int}} = p_s \cdot s \qquad (1)$$

where p_s is the surface minority carrier density of holes in the silicon, assuming no band bending.

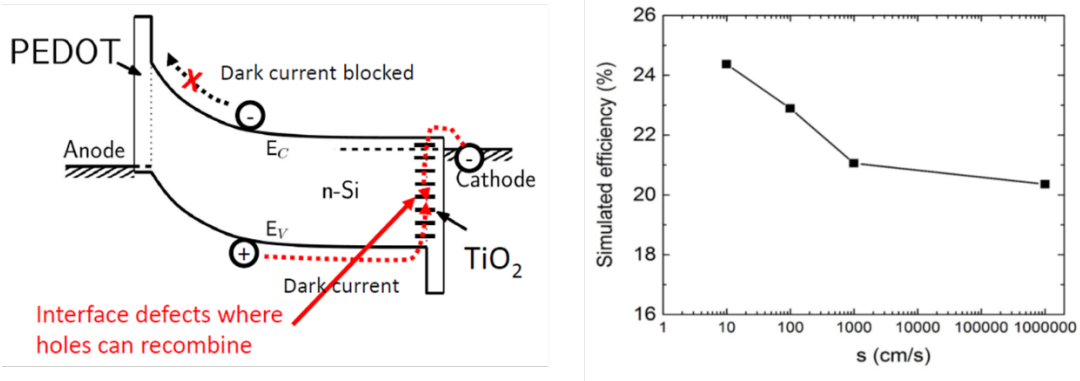

Figure 3. (a) Process of recombination at the Si/ TiO_2 interface states, which leads to hole current, increasing dark current and degrading open-circuit voltage, and (b) simulated cell efficiency as a function of recombination velocity s at the Si/ TiO_2 interface.

For example, if no barrier were present, the holes would recombine nearly instantly at the Si/metal interface, with a near-infinite recombination velocity (found to be ~10^7 cm/s in practice). High quality Si/SiO_2 interfaces (from thermal oxide grown at ~1000 ^oC) with forming gas annealing can have a recombination velocity ~ 100 cm/s, with record low values ~10 cm/s. Modeling in this project shown in Figure 3 (b) shows the effect of this rear interface recombination on maximum cell efficiency (by affecting the dark current) for a cell with thickness ~300 um. Surface recombination velocities less than 100 cm/s are clearly desired, with ~10 cm/s as an ultimate target.

I.C. Comparison to Silicon "HIT" cells

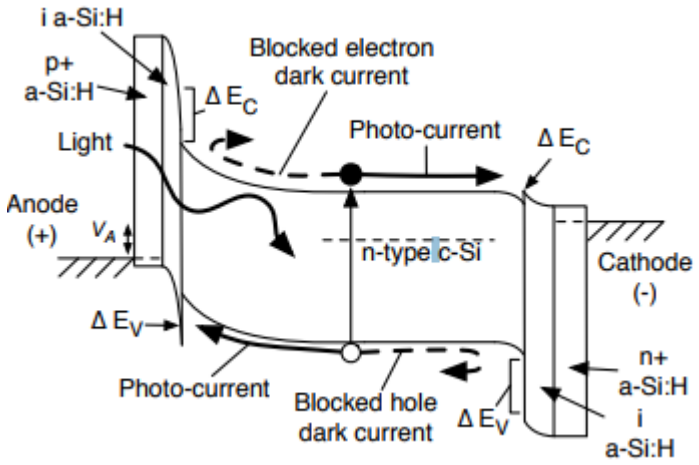

Figure 4. Band structure of "HIT" silicon solar cell, with efficiencies > 25% . The intrinsic amorphous silicon layer passivates the silicon surface, and the doped layer helps set the quasi-fermi levels. Note the similarity to the structure of Figure 1(b).

The highest efficiency crystalline silicon solar cells to date (>25%) are the 'Heterojunction with Intrinsic Thin layer' (HIT) structure which uses heterojunctions formed between amorphous silicon and crystalline silicon (Figure 4). A high-lifetime crystalline silicon substrate forms the base and absorbing layer of the cell. The thin layers of amorphous

silicon are deposited on the two sides of the crystalline silicon substrate using Plasma Enhanced Chemical Vapor Deposition (PECVD) at temperatures ∼200-300 ◦C. Amorphous silicon has a bandgap much larger (~1.7 eV) than that of crystalline silicon. In modern HIT solar cell structures, a thin layer of intrinsic amorphous silicon is used as a passivation layer, and a heavily doped amorphous silicon layer is added to achieve carrier selectivity [Keiichiro Masuko, et al. "Achievement of More Than 25 Percent Conversion Efficiency With Crystalline Silicon Heterojunction Solar Cell. IEEE Journal of Photovoltaics, 4(6):1433–1435, (November 2014)]. Note that the band diagram of such cells is very similar to that of our proposed structure (Figure 1(b)).

As in our proposed structure, in the HIT cell there are no extra doped layers on either substrate surface beyond the substrate doping, and hence Auger effects and bandgap narrowing mentioned are avoided. Recent modelling of such cells with 25.1% efficiency shows that surface recombination velocities at each of the two selective contacts, $s = W/(2\ \tau_{surf}$, as in Eq'n (4), Sect IV)), are under 10 cm/s [(D. Adachi et al, Appl Phys. Lett. vol 107, 23506 (2015)], as expected from Figure 3. Our proposed work has the potential advantages that a simple CVD growth process, as described in the next section, could be easier and lower-cost to scale to large area than the PECVD process used in HIT cells for amorphous silicon. Further, any parasitic absorption in the doped layers might be avoided.

I.D. Summarizing this section:

- We seek a double-heterojunction solar cell architecture on high lifetime silicon to retain the high-efficiency of silicon cells and to reduce their cost.
- Low temperature methods to deposit the hole and electron barriers could reduce cost compared to high-temperature diffusions

- This project will focus on the growth of TiO_2, its fundamental properties, and applications to PV.
- Low interface recombination at Si/TiO_2 is critical.

II. Task 1: Synthesis and Interface Bonding of Hole-Blocking Semiconductor on Silicon: TiO_2

II.A. Growth of TiO_2 on Silicon from titanium(IV) tetra-(tert butoxide) and Film Properties

Results in this section are published in part in:

S. Avasthi, W. E. McClain, G. Man, A. Kahn, J. Schwartz, and J. C. Sturm, "Hole-blocking titanium-oxide/silicon heterojunction and its application to photovoltaics," Applied Physics Letters, vol. 102, (2013). doi: 10.1063/1.4803446

J. Jhaveri, S. Avasthi, G. Man, W. E. McClain, K. Nagamatsu, A. Kahn, J. Schwartz, and J. C. Sturm, "Hole-blocking crystalline-silicon/titanium-oxide heterojunction with very low interface recombination velocity," in 2013 IEEE 39th Photovoltaic Specialists Conference (PVSC), ed, 2013, pp. 3292-3296. doi: 10.1109/PVSC.2013.6745154

K. Nagamatsu, Crystalline Silicon Photovoltaics via Low-Temperature TiO_2/Si and PEDOT/Si Heterojunctions, Ph.D. Thesis, Princeton University, January, 2016. (http://www.princeton.edu/sturm/publications/phd-theses/)

Growth of TiO2 from titanium(IV) tetra-(tertbutoxide)

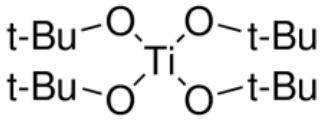

Figure 5. Diagram of bonding in Titanium tetra-(tert-butoxide) precursor molecule.

The deposition process used in this work is similar to atomic layer deposition (ALD) in that it is used to deposit nanometer thick layers using an adsorbed precursor; however, there are two notable differences. First, unlike ALD, the process does not use a second reactant, such as

water, to react with the Ti precursor to form titanium dioxide. The metal-organic precursor used was titanium(IV) tetra-(tert-butoxide) or $Ti[OC(CH_3)_3]_4$, which is shown in Figure 5, contains both the Ti and O atoms. This simplifies the deposition system, in that no bubblers or high-speed isolation valves are required. Second, unlike ALD precursors, like titanium tetrachloride, titanium(IV) tetra-(tert-butoxide) is not intrinsically self-limiting. This leads to a deposition regime where more than one monolayer can be deposited in one cycle. Due to the two differences, our deposition process is better described as a modified CVD process. The process also differs because of the relatively low-temperatures used; the maximum temperature reached is ~ 100 ◦C, in contrast to conventional CVD of TiO_2 which can reach 275 ˚C to 675 ˚C.

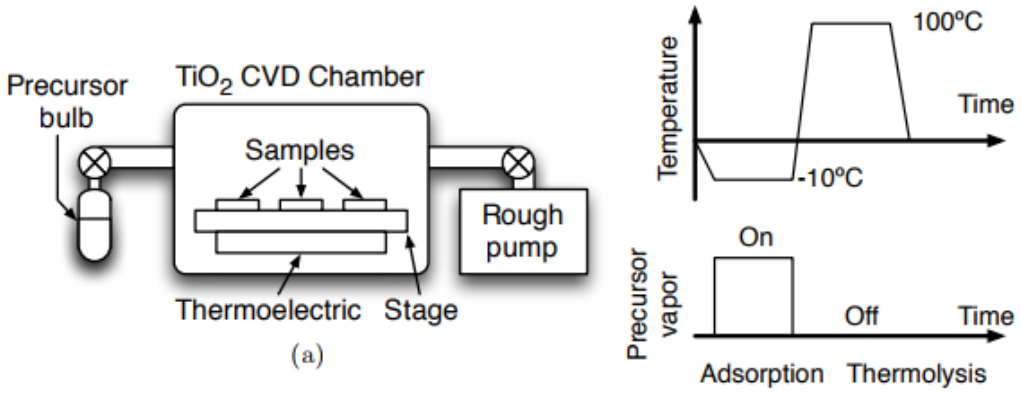

Figure 6. Illustration of (A) TiO_2 deposition chamber and (B) temperature and precursor setting for one cycle.

In concept the TiO_2 deposition system is very simple and involves a minimal number of components, as illustrated in Figure 6(a) and Figure 7. The main chamber contains a stage with a thermoelectric device for heating and cooling. A mechanical roughing pump is connected to one end of the chamber. On the other end, a valve connects the chamber to a vial of the precursor liquid. The surface area of the precursor vial was ~ 3 cm^2. The main

chamber also has a nitrogen inlet for venting purposes and a window for observation of samples during depositions.

The fabrication sequence begins with cleaning of an electronic-grade, polished silicon sample. The cleaning process involves a solvent cleaning procedure and an RCA clean. Immediately before entering the TiO_2 deposition chamber, a dip in 20:1 H2O:HF acid for 1 minute is performed to remove any oxides and form a hydrogen-terminated silicon surface . After samples are placed in the chamber, it is pumped down to a base pressure of 20 mtorr to 50 mtorr and the chamber remains pumped for the remainder of the deposition.. The samples are first cooled by the thermoelectric stage to −10 ◦C, and the samples are then exposed to vapor from the precursor vial. The standard length of the adsorption step used is 10 min. The cooling of the sample stage facilitates adsorption of a thin layer of Ti-alkoxide on the samples. Because the precursor adsorbs on the stage as well, a thin layer of precursor also wicks underneath the samples, so that adsorption occurs on both sides of the sample. The growth process is not performed one atomic layer at a time, in contrast to ALD, because more than one monolayer of the alkoxide is adsorbed onto the sample during the cooling step. After adsorption, the samples are heated to 100 ◦C for 10 min in order to thermolyze the alkoxide. The thermolysis step serves to break the iso-butene from the titanium, leaving hydroxyl groups that condense to give a stoichiometric TiO_2 film with elimination of water. Because the alkoxide adsorbs to both surfaces of the sample (top and bottom), TiO_2 is obtained on both surfaces. The adsorption and thermolysis steps comprise one cycle, and a standard deposition uses three cycles, which results in a film thickness of 2 nm to 3 nm. (Some early work (Version 1 reactor) did not have a thermoelectric stage, and samples were heated and cooled by dry ice or heat outside the quartz deposition tube.)

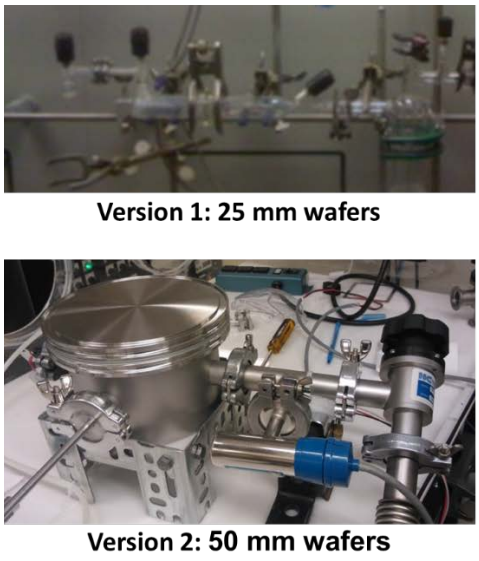

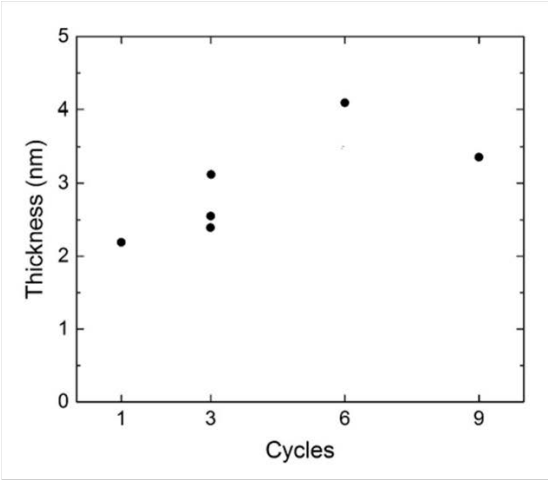

(a) (b)

Figure 7. (a) Pictures of growth reactors, with most results in this report from Version 2. (b) TiO_2 thickness by spectroscopic ellipsometry vs. number of deposition cycles, for adsorption time of 10 min and temperature of -10 ^oC.

The film thickness saturated after about 3 cycles for 10 min precursor adsorption time and -10 ^oC adsorption temperature. In a separate set of experiments, increasing the absorption time and varying the absorption temperature had little effect (Figure 8). The following section describes modifications to growth thicker TiO_2.

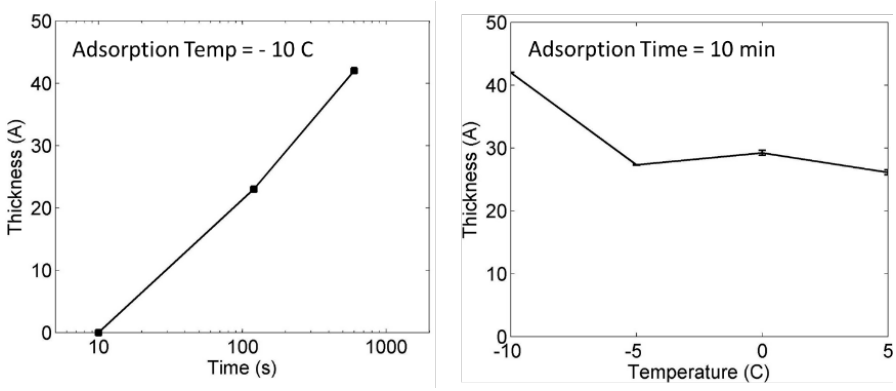

Figure 8. TiO_2 thickness for a 3-cycle run vs. precursor adsorption time and vs. adsorption temperature.

Modified Growth Process for Thicker TiO_2

The first approach to grow thicker layers was to simply increase the number of adsorption and thermolysis cycles used in the low-temperature CVD process described above. The hypothesis was that more of the titanium alkoxide precursor would adsorb and thermolyze with each subsequent cycle, increasing the thickness of the overall film. In this approach, samples are placed into the chamber and undergo a set amount of repeated cycles before removal. However, the thickness of TiO_2 layers obtained by simply increasing the number of cycles was observed to saturate, as shown by Figure 7 and Figure 9. It is hypothesized that the presence of unreacted organic groups left from incomplete decomposition of the precursor on the surface of the TiO_2 film can prevent the adsorption of more precursor. If no precursor molecules adsorb to the surface of the film, then there is no TiO_2 created during the thermolysis step and the thickness of the film does not increase with further cycling. As a result, the growth of the TiO_2 films is observed to saturate at ~3 nm to 4 nm.

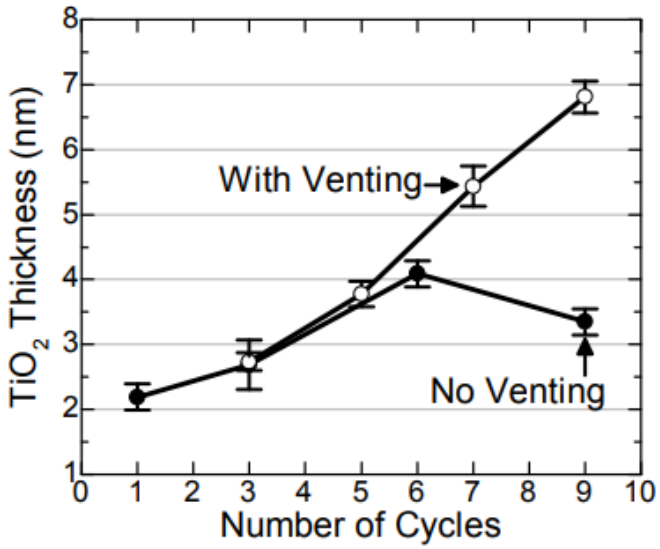

Figure 9. Thickness of TiO_2 films versus number of cycles using venting process (hollow circles) and without venting (filled circles).

To facilitate decomposition of the organic groups that may be present on the surface of the TiO_2 film, the introduction of oxygen and water vapor from laboratory ambient was investigated. Since the titanium(IV) tetra-(tert-butoxide) precursor is quickly broken down upon exposure to oxygen and water vapor, it was hypothesized that exposure to laboratory ambient would allow unreacted organic groups on the surface of the TiO_2 film to decompose. By reacting the surface organic groups, the titanium alkoxide should then be able to adsorb to the TiO_2 surface, resulting in more TiO_2 deposition upon further cycling. Laboratory ambient was introduced by venting the deposition chamber between cycles, as shown schematically in Figure 9. After a number of cycles (typically 3), the chamber is vented and exposed to laboratory ambient for 1 min to 5 min. Then the chamber is pumped back down and additional cycles are run to add thickness to the TiO_2 film. Venting the chamber was observed to prevent the saturation of TiO_2 thickness with additional cycles. For the data shown, 3 cycles were run for the initial TiO_2 film, which resulted in ~2.7 nm thickness. By venting the chamber and then running an additional 2 cycles, the thickness was increased to ~3.8 nm, then ~5.5 nm, and finally a ~6.8 nm film was achieved. However, note that XPS of these films showed a signal which could not be clearly identified, leading us to speculate that such films had some contamination (perhaps from the air).

Another variation used in some experiments for band-offset measurements (Task 2) used a single controlled pulse of vapor pressure from the precursor vial to obtain thicker TiO_2 growth. A vial with larger surface area (~10 cm^2) was used. The process nominally follows the same procedure as the standard method described above, yet with a precursor valve that can be carefully controlled. This method controls the opening speed of the precursor bulb in order to obtain a spike in the chamber base pressure. It is hypothesized that the spike in pressure is due to a burst of precursor vapor entering the chamber, which results in a thick coating of adsorbed precursor onto

the samples. As a result, this method is observed to obtain TiO_2 films that are 5 nm to 12 nm thick, depending on location within the chamber. Significantly, no "contamination" signal from XPS was observed in such layers with the single-pulse process.

Film Characterization

The thickness of the titanium dioxide layers was measured by ellipsometry in a Gaertner Stokes Ellipsometer LSE. The system used a 632.8 nm laser at two angles to yield both thickness and refractive index. Measurements were taken at 5–10 different spots on the sample. The titanium dioxide layers were found to be 1–4 nm thick, with a standard deviation of less than 5%. The refractive indices of the deposited films were usually around 2.2–2.7. These values are comparable to the refractive index of titanium dioxide in the rutile phase, suggesting that the deposited films are relatively dense.

To investigate the morphology and texture of the deposited titanium dioxide layers, atomic force microscopy (AFM) measurements were done on a Dimension Nanoman (Veeco Instruments). AFM reveals an extremely smooth and conformal film with a RMS roughness of only 0.5 nm (image not shown here) over a scan area of 50 um x 50 um. No long-range features or cracks are observed anywhere on the surface (sample size is 1.6 cm x 1.6 cm). Also of interest is the crystallographic nature of the titanium dioxide film. If present, grain boundaries in a polycrystalline titanium dioxide layer would be visible in the phase image of atomic force microscopy. In the phase image of our film, no grain boundaries are visible (RMS = 0.94^o), suggesting that the titanium dioxide layer is amorphous and not polycrystalline. The lack of crystal boundaries is in contrast to previously reported results where the anatase phase has been observed

at deposition temperatures above 275 °C. We speculate that the lack of crystallinity in our titanium dioxide layer is due to the much lower deposition temperature (100 °C).

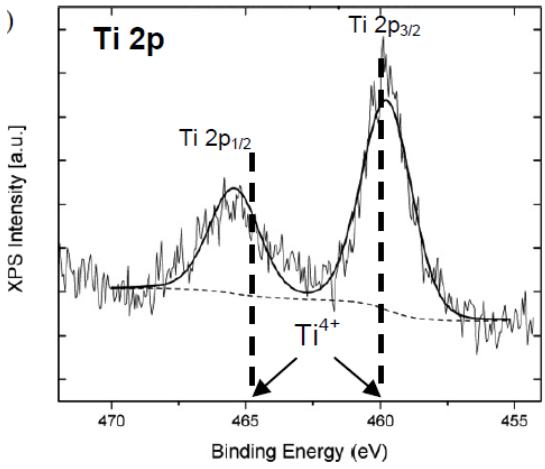

Figure 10. XPS spectrum of TiO_2 layers deposited from titanium(IV) tetra(tert-butoxide) on Si and annealed at 100 °C.

To confirm the presence of a titanium dioxide layer and to investigate the chemical oxidation state of the titanium atoms, X-ray photoelectron spectroscopy (XPS) was used (Figure 10). For the XPS measurements, titanium dioxide was first deposited on a highly doped p-Si (< 0.005 Ohm-cm). Samples were then transported in air to the measurement system. The XPS measurements were performed in a dedicated UHV chamber. Al kα radiation at 1486.6 eV was used in XPS, with an experimental resolution of 0.5 eV. The measured Ti_{2p} spectrum (Figure 10) shows two peaks at binding energies of 459.7 and 465.3 eV. The peak position of $Ti_{2p3/2}$ at 459.7 eV compares well to the peak position for $Ti2_{p3/2}$ for Ti^{4+} in TiO_2 (458.6–459.2 eV), and is significantly different from the $Ti_{2p3/2}$ peak of Ti^{2+} (454.9–455.2 eV) and Ti^0 (453.7–454.2 eV). The intensities of the peak at 459.7 eV and 465.3 eV have a ratio of 2.2:1, close to the branching ratio of 2:1 expected for the 2p lines. Finally, the measured spin-orbit splitting is 5.6 eV, which

compares more favorably to the spin-orbit splitting of Ti^{4+} (5.5 eV) rather than to the spin-orbit splitting of Ti^{0} (6.2 eV). In summary, the XPS measurements confirm the presence of titanium dioxide on the surface.

Next, to measure the bandgap and band-alignment at the Si/TiO_2 interface, we used ultra-violet spectroscopy (UPS) and inverse-photoelectron spectroscopy (IPES). The UPS measurements used the He I line (21.22 eV) of a gas discharge source, and IPES used a commercial electron gun and a fixed photon energy detector (centered at 9.2 eV). Figure 11(a) shows a combined UPS and IPES spectrum of Si/ TiO_2 interface as a function of the binding energy. UPS provides the valence band edge, which is found to be at 3.8 eV below the Fermi level. While IPES probes the conduction band edge, which is shown to be 0.8 above the Fermi level. The resulting band gap of the TiO_2 layer is hence 4.6 eV. This value is much bigger that the 3.8 eV reported for crystalline TiO_2 (rutile phase). This could be either the result of the TiO_2 layer being extremely thin or the TiO_2 layer being amorphous.

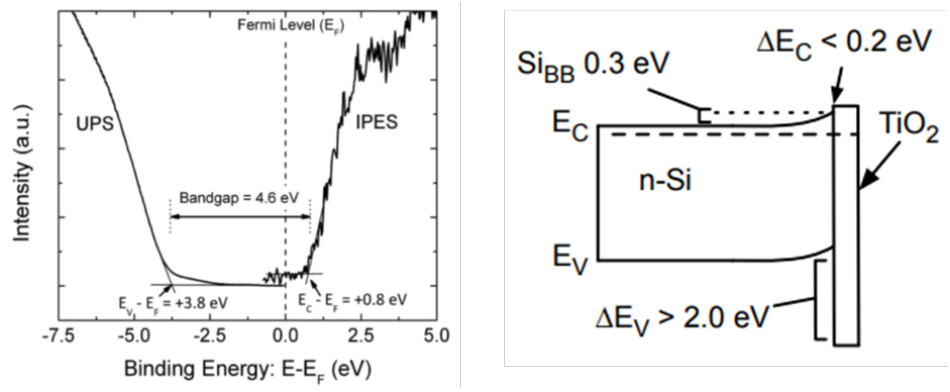

Figure 11. (a) Combined UPS and IPES spectrum of TiO_2 on p^+ Si, showing the bandgap of TiO_2 layer, and (b) energy band diagram showing offsets on n-type silicon.

Figure 11(b) shows a typical band alignment from UPS and IPES on n-type silicon. A small conduction band offset and large valence band offset are observed, both as desired for the

hole-blocking / electron-selective contact. A band-bending in the silicon, indicating depletion near the surface, was also observed. This would lead to minority carriers being attracted to the surface, leading to a low interface recombination velocity, the opposite of what is desired. Much more extensive measurements and comments are made in Task 2 (Band Alignments).

II.B. Interface Bonding and Structure

Results in this section are published in part in

G. Sahasrabudhe, S. M. Rupich, J. Jhaveri, A. H. Berg, K. A. Nagamatsu, G. Man, Y. J. Chabal, A. Kahn, S. Wagner, J. C. Sturm, and J. Schwartz, "Low-temperature synthesis of a TiO_2/Si heterojunction," Journal of the American Chemical Society, vol. 137, pp. 14842-14845 (2015). doi: 10.1021/jacs.5b09750

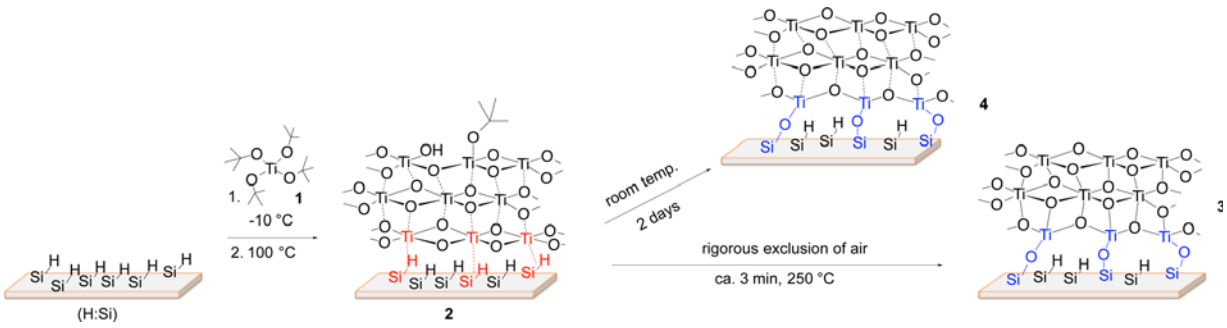

Figure 12. Scheme 1: Titanium tetra(tert-butoxide), 1, is deposited on a cooled (−10 °C) sample of H-terminated Si and then heated at 100 °C to give 2. Preparing 3 from 2 in the absence of air obviates formation of SiOx and enables identification of Si−O−Ti interfacial species. No structure for "Si−H" is implied.

The TiO_2 layer in this section was synthesized (Scheme 1 in (Figure 12)) by vapor phase deposition of titanium tetra(*tert* butoxide) (1) onto the externally cooled substrate at 10^{-3} Torr; it was then heated to 100 °C, briefly exposed to air at room temperature, and then used (as 2) for device fabrication To understand at the molecular level the role played by the TiO_2/H:Si interface in our devices, we examined speciation for 2 and its thermal evolution products 3 and 4 by angle-resolved X-ray photoelectron spectroscopy (XPS). Our efforts might have been

compromised, however, by the possible formation of silicon oxide (SiO_x) formed during the brief periods of air exposure attendant to our procedures. To obviate SiO_x in order to unambiguously identify interfacial speciation, we repeated our synthesis procedures, but with rigorous exclusion of air.

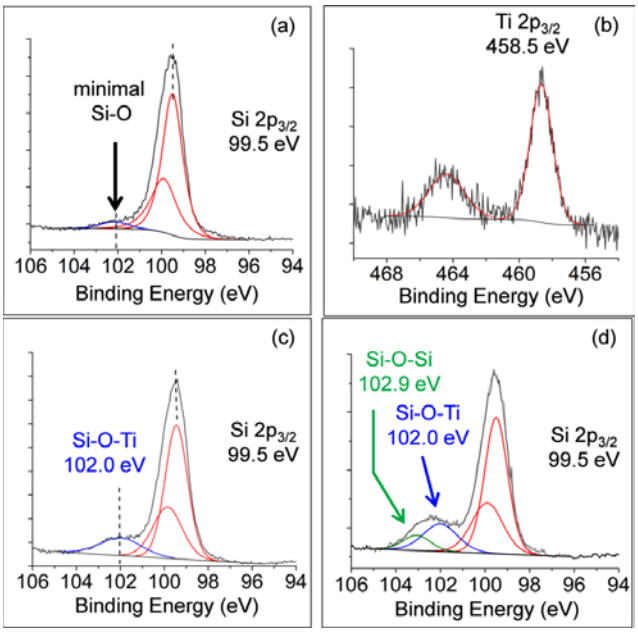

Figure 13. Angle-resolved XP spectra taken at 70° from surface normal (a) Si(2p) for 2; (b) Ti(2p) for 2; (c) Si(2p) for 3; (d) Si(2p) for 2 exposed to air for 30 min and then heated to 250 °C. The y-axis scale represents arbitrary counts.

In a typical "no air" experiment Si(100) wafers were cleaned by standard methods and then dipped in a 20:1 deionized water: 48−50% aqueous hydrofluoric acid solution for 45 s to give hydrogen terminated silicon (H:Si). The substrate was rinsed with Milli-Q water, dried, and placed in a glass tube that was connected to both a reservoir of the titanium tetra(tert-butoxide) (1) precursor of TiO_2 and to vacuum; it was then externally cooled to −10 °C and exposed to vapor of 1 (Scheme 1) for 10 min at 10^{-3} Torr. The substrate was next heated at 100 °C for 10 min to form TiO_2/H:Si (2) and was then cooled to room temperature. The TiO_2-coated substrate was then transferred in the sealed deposition chamber into a nitrogen atmosphere glovebox from

which it was transferred into the antechamber of the XPS spectrometer via a “vacuum suitcase” that precludes air intrusion. A second sample was heated in the glovebox to 250 °C on a hot plate (to give 3) and was subsequently transferred into the antechamber, also via the “suitcase.” XPS analysis of 2 showed the binding energy for Ti(2p) (Figure 13b) to be typical of Ti(IV), with no discernible signal for any lower valent Ti species; essentially no peak for Si−O was seen in the angle-resolved Si(2p) XP spectrum (Figure 13b), though the C(1s) spectrum showed some tert-butoxy groups are still present. We suggest that the TiO_2 is formed by stepwise dehydration at 100 °C in which tert-butoxy groups thermolyze to 2-methyl-1-propene with concomitant formation of Ti−OH groups; these condense with elimination of water to give the Ti−O−Ti moieties of 2 (Scheme 2 in Figure 14).

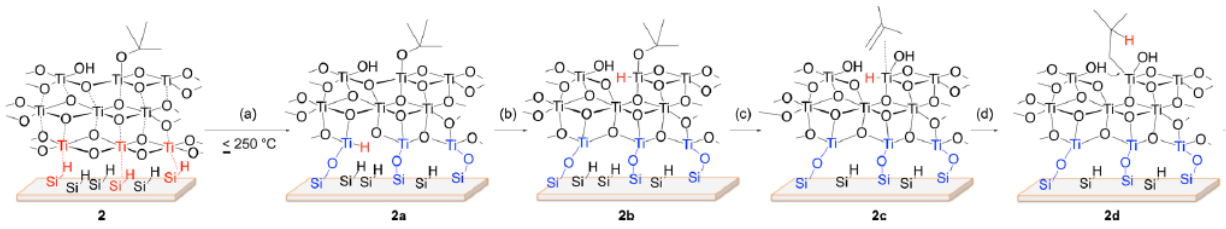

Figure 14. Scheme 2: Proposed formation of Si−O−Ti in the absence of air by a sequence of (a) Si−H/Ti-O σ-bond metathesis, (b) H−Ti/O-Ti σ-bond metathesis, (c) tert-butoxy ligand fragmentation, and (d) β-hydride addition and protonolysis by a neighboring Ti−OH moiety.

Heating 2 to 250 °C may further cross-link the TiO_2 to give 3; 2 exfoliates in water, but 3 does not. XPS analysis of 3 showed no change in the Ti(2p) spectrum, but a new signal appeared for Si(2p) (Figure 13c). Since 3 had never been exposed to air, this new peak must derive from reaction between a surface Si species and the TiO_2 overlayer. Angle-resolved XPS showed that this new species is surface-located; the depth of this Si−O layer is 2− 3 Å. Its binding energy, BE = 102.0 eV, is lower than that for SiO_x (BE = 102.7−103.0 eV). We assign it to a new interfacial species, Si−O−Ti; this lower BE assignment is consistent with the lower

electronegativity of Ti vs Si. This same Si(2p) spectrum was recorded for 2, which was stored under inert atmosphere for 2 days to give 4 . As a control, H:Si was heated at 250 °C for 5 min in the absence of air; no Si−O species were observed in the XPS .

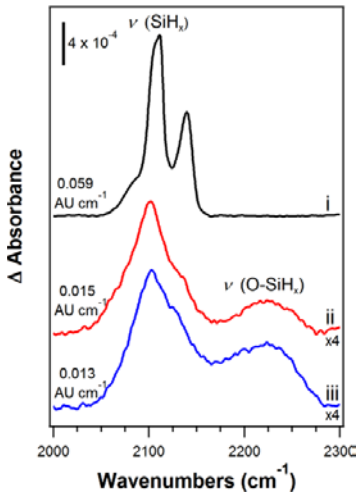

Figure 15. Attenuated total reflectance-FTIR absorption spectra of (i) an H-terminated Si(100) surface; (ii) 3, with no air exposure; and (iii) 3, after 18 h air exposure. All spectra were referenced to a clean, chemically grown oxide on Si(100). The area of the SiH_x peaks were integrated over the region from 2040 to 2165 cm−1. Spectra ii and iii are magnified ×4 for clarity.

All Ti and Si peak positions and intensities in XP spectra of 3 remained unchanged after 18 h of ambient exposure. In contrast, when 2 was exposed to air for only 30 min prior to heating at 250 °C, Si(2p) XPS showed a broad peak, which could be deconvolved into a component assigned to Si−O−Ti and a second one to SiOx (Figure 13d) consistent with some Si−H oxidation.

We propose that Si−O−Ti formation under anaerobic conditions involves σ-bond metathesis between surface Si− and Ti−O groups of the TiO_2 overlayer, which yields a Ti−H species (intermediate 2a in Figure 14); such ligand exchange is well established for the titanium alkoxide-activated reduction of organics using polymeric hydrosiloxanes. Further H−Ti/O− Ti

σ-bond metathesis (to 2b), thermal decomposition of tertbutoxyl ligands to Ti−OH and 2-methyl-1-propene (2c), and finally Ti−OH protonolysis of the (2-methylpropyl)titanium resulting from β-hydride addition (2d) gives the observed products (Scheme 2).

ATR-FTIR further probed the effect of TiO_2 film formation on the Si−H surface: Differential absorption spectra of the starting Si−H surface (Figure 15,i) and 3 before (Figure 15,ii) and after 18 h of ambient exposure (Figure 2,iii) were referenced to a clean, chemically oxidized surface. About 25% of initial Si−H was found to remain by comparison of peak areas for the SiH_x region (2050−2150 cm^{-1}) after TiO_2 deposition. A small shoulder at ca. 2260 cm^{-1} appears and is assigned to the stretching mode of Si−H where oxygen is "back-bonded" to Si; this shoulder grew with exposure to air. The persistence of Si−H bonds in 3 can be understood by comparing the areal density of Si atoms in the Si(100) plane (ca. 7×10^{14} Si atoms/cm^2) compared to that of Ti atoms in a model (rutile) TiO_2 (111) plane (ca. 5×10^{14} Ti atoms/cm^2). Thus, the Ti in 3 can bond to only about 70% of the Si atoms by this analysis, leaving about 30% of the original Si−H bonds unreacted (Scheme 1), approximating our experimental result. The TiO_2 film of 3 acts somewhat as a protective layer, slowing air oxidation of residual Si−H bonds, consistent with XPS observations.

The purpose of TiO_2 films that are grown on n-type Si in a device is to let electrons pass and to reflect photoexcited holes in order to raise the photovoltage of solar cells. The maximum photovoltage is generated when all holes that impact a TiO_2/n-Si interface reflect from it without recombining. At nonideal interfaces some holes do get trapped in interface defect states and then recombine with electrons; the rate of this recombination rises with the areal density of interfacial electronic defects, which are associated with incomplete bonding across the interface. The effective lifetime (τ_{eff}) of holes is reciprocal to the surface recombination velocity (SRV): the

lower the SRV, the longer the effective hole lifetime. The τ_{eff} for 2 was measured by the quasi-steady state photoconductance decay (QSSPCD) method as in the previous section to be poor, with SRV > 1000 cm/s. In marked contrast, τ_{eff} for 4 was measured to yield an SRV as low (good) as 30-50 cm/s (see Task 3), comparable to lifetimes reported for TiO_2/Si heterojunctions made by low temperature atomic layer deposition (ALD) or sol−gel type processes. The τ_{eff} for 3 also yielded a good SRV (ca. 50 cm/s). In short, the SRV depends critically on the chemical nature of the TiO_2/Si interface: In the absence of Si−O−Ti bonding (2), τ_{eff} is unfavorably short; when Si−O−Ti bonding is present at the interface (3 and 4), τ_{eff} can be improved significantly.

II.C. Task Summary

- We developed a novel growth process for TiO_2 on silicon, using a single precursor (titanium(IV) tetra-(tert-butoxide) or $Ti[OC(CH_3)_3]_4$) for process simplicity
- The maximum process temperature of 100 ^oC is lower than any other known CVD or ALE method.
- The films are smooth and probably amorphous
- The band offsets and TiO_2 bandgap are as expected from Figure 2, but the silicon band-bending needs further investigation.
- A TiO_2/Si interface that comprises Si−O−Ti bonding is of high electronic quality and can be prepared at surprisingly low temperatures compared to the standards of classical silicon technology. This interface has an extremely low density of electronically active defects, as shown by our measurements of effective lifetimes.

- We attribute this in part to the Si-O-Ti interface bonding analogous to the Si-O-Si bridging oxygen between the Si and SiO_2 layers in standard silicon MOS technology, although not all surface Si has such structure.
- The long-term degradation in air of effective surface recombination velocity (Task 3) maybe the oxidation of Si-H on the Si surface

III. Task 2: Heterojunction Formation and Band Alignments at the TiO_2/Silicon Interface

The work in this section was published in part in:

G. Man, J. Schwartz, J. C. Sturm, and A. Kahn, "Electronically Passivated Hole-Blocking Titanium Dioxide/Silicon Heterojunction for Hybrid Silicon Photovoltaics," Advanced Materials Interfaces, vol. 3, pp. 1600026 (2016). doi: 10.1002/admi.201600026

With the present study, our aim is to provide an in-depth investigation of the electronic band alignment and electrical transport properties of the aforementioned TiO_2/c-Si heterojunction with as-deposited TiO_2 layers. The combined interface and device study of the abrupt, interfacial layer-free TiO_2/c-Si heterojunction demonstrates the absence of interface Fermi level pinning, a characteristic of an electronically passivated interface. Simple Fermi level equilibration is revealed to be the driving mechanism behind the energy level alignment.

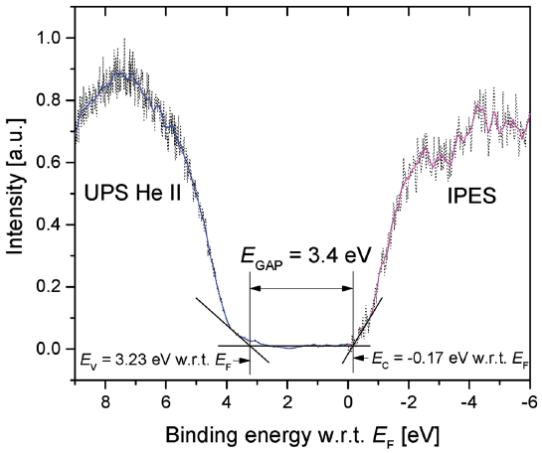

Figure 16**.** Combined UPS Helium II and IPES spectra of as-deposited TiO_2 , showing the transport gap E_{GAP}. The energy reference (0 eV) corresponds to the position of the Fermi level E_F.

III.A. Band Positions and Electronic Structure

The electronic structure of as-deposited TiO_2 films is investigated using a combination of ultraviolet photoemission spectroscopy (UPS) and inverse photoemission spectroscopy (IPES) (Figure 16). Our previously published work showed UPS Helium I and IPES spectra measured on 1–4 nm thick TiO_2 on Si. [Jhaveri et al, IEEE PVSC (2013)]. Both spectra included some contributions from the underlying silicon, which complicated the determination of the valence and conduction band edges of TiO_2. The development of a process for depositing thicker (10–15 nm) TiO_2 films, coupled with the use of more surface-sensitive UPS Helium II (as compared to Helium I), enables a more accurate determination of the electronic structure of TiO_2 . Under typical deposition conditions, TiO_2 is an n-type material doped by oxygen vacancies (deep donors) and/or titanium interstitials (shallow donors). This is confirmed here by the position of the Fermi level (E_F) close to the conduction band minimum E_C (TiO_2). The work function of as-deposited TiO_2, $\varphi(TiO_2)$, measured from the photoemission cut-off (not shown here), is 4.0 ±0.1 eV. The valence

band maximum E_V (TiO_2) is at 3.2 eV below E_F, giving an ionization energy of 7.2 ±0.2 eV. Conversely, E_C (TiO_2) is at 0.2± 0.2 eV above *E* F, giving an electron affinity (EA) of 3.8 ±0.3 eV and a band gap of 3.4 ±0.3 eV. Tezuka et al. [J. Phys. Soc. Jpn. 74 (1994)] previously used a combination of X-ray photoemission spectroscopy (XPS) and IPES to establish a band gap of 3.3 ±0.5 eV for rutile TiO_2. Although there is a spread of values in the literature, the general consensus is that the band gaps of crystalline rutile and anatase TiO_2 are 3.03 and 3.20 eV, respectively. The slightly larger band gap reported in this work could be due to the noncrystalline phase of the as-deposited TiO_2, which is grown at a maximum temperature of 100 ^oC. Typical amorphous-to-crystalline-anatase transitions occur at ~300 ^oC. A small density of states extending above E_V (TiO_2) into the gap corresponds to tail states, which can also be seen in the optical absorption spectra of TiO_2 on glass (Figure 17).

A 3.42 eV optical gap is extracted from the absorption spectrum of TiO_2. This value compares well to the above transport gap (3.4 ±□0.3 eV), since the exciton binding energy in (rutile) TiO_2 is on the order of 5 meV [Landolt-Börnstein—Group III Condensed Matter 41D (Non-Tetrahedrally Bonded Binary Compounds II), No. 41D (Eds: O. Madelung, U. Rössler, M. Schulz), Springer-Verlag, Berlin, 2000]. The magenta fit in Figure 17 corresponds to the expected spectrum if the optical absorption originated solely from an interband transition. [J. Pankove, Optical Processes in Semiconductors , Dover Publications Inc., New York, NY, 1975] However, as the actual spectrum shows, there is substantial subgap absorption due to a distribution of tail/defect states.

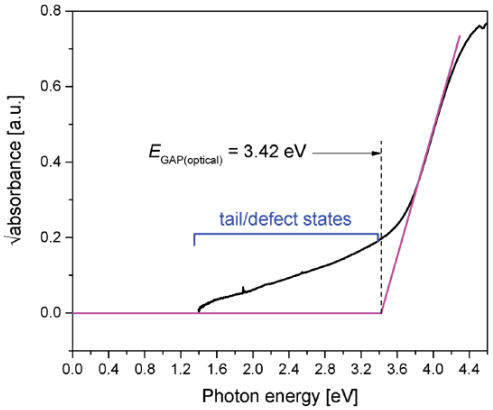

Figure 17. UV–vis absorption spectra of ~5 nm of as-deposited TiO_2 on glass, showing the optical gap E_{GAP}(optical)

XPS was used to probe the chemical composition of the TiO_2/Si interface. The silicon 2p (Si2p) core level spectra for various TiO_2/Si heterojunctions, featuring n-Si and p-Si ranging in doping concentration from 10^{16} to 10^{19} cm^{-3}, are shown in Figure 18a. The Si2p peaks were fitted with 20% Lorentzian, 80% Gaussian peaks with a spin–orbit splitting of 0.4 eV between the $Si2p_{1/2}$ and $Si2p_{3/2}$ peaks. The $Ti2p_{1/2}$ and $Ti2p_{3/2}$ components were fitted with the same Lorentzian:Gaussian ratio as the Si2p peaks, and a spin–orbit splitting of 5.54 eV [J. Moulder, W. Stickle, P. Sobol, K. Bomben, Handbook of X-Ray Photoelectron Spectroscopy, Physical Electronics, Inc., Eden Prairie, MN, 1995]. The Ti2p core level spectra (Figure 18b) indicates that titanium is in its +4 oxidation state, as shown above in Task 1 [S. Avasthi, W. E. McClain, G. Man, A. Kahn, J. Schwartz, J. C. Sturm, Appl. Phys. Lett., vol. 102, 203901 (2013)]. In all cases, the Si2p peak corresponding to bulk silicon dominates the spectra, indicating that the interface has not undergone a chemical reaction and is spatially abrupt. This is in contrast with TiO_2/Si interfaces formed via less gentle and higher temperature processes, which have shown the presence of combinations of titanium silicides, titanium oxides, and silicon oxides of various stoichiometries [L. J. Brillson, M. L. Slade, H. W. Richter, H. VanderPlas, R. T. Fulks, J. Vac. Sci. Technol. A, 4,

993 (1986)]. Schlom et al. state that a chemical reaction between Si and TiO_2 is energetically favorable since the volume free energy change ΔG is negative [D. G. Schlom, C. A. Billman, J. H. Haeni, J. Lettieri, P. H. Tan, R. R. M. Held, S. Volk, K. J. Hubbard, in Thin Films and Heterostructures for Oxide Electronics (Ed: S. B. Ogale), Springer, pp. 31 – 78, New York, NY, 2005]. This suggests that irrespective of how the interface is formed, a chemical reaction will occur at higher temperature. Indeed, our own experiments on the TiO_2/Si heterojunction show evidence for Si-O-Ti bonding at the interface (previous section), after the heterojunction is annealed at 250 ^oC for 3 min in an inert atmosphere. The formation of a mixed silicon/ titanium oxide interfacial layer appears to be kinetically limited.

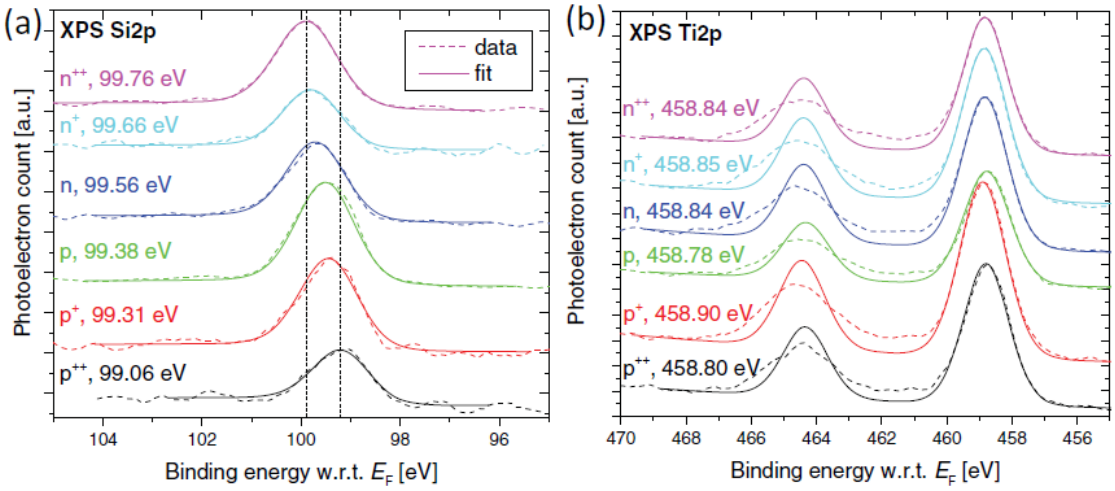

Figure 18. XPS spectra of the a) silicon 2p and b) titanium 2p core levels, for as-deposited TiO_2 on a variety of n-Si and p- substrates. The peak positions are given for the Si and $Ti_{2p\ 3/2}$ peaks. The data are plotted in dashed lines, and the peak fits are represented by solid lines.

III.B. Band Alignments

XPS was also used to elucidate the electronic band alignment at each TiO_2/Si heterojunction using the Kraut method. Indeed, the short mean free path of UPS photoelectrons precludes the direct measurement of the Si valence band edge through the TiO_2 layer, and use is made of the larger probing depth of XPS for the Si 2s and 2p core levels. First, the spatial region probed by the

XPS measurements must be clarified. At the soft X-ray photon energy used (1486.7 eV), photoelectrons originating from the Ti2p and Si2p core levels have kinetic energies of ~1000 and ~1400 eV, respectively. From the standard universal curve of inelastic mean free path (IMFP) versus electron kinetic energy, the IMFPs of Ti 2p and Si 2p photoelectrons are ~2 and ~2.5 nm, respectively. Attenuation of the photoelectron signal follows an exponential distribution into the solid, starting at the free surface of the solid. In essence, XPS Ti2p measurements probe the topmost ~4 nm of the TiO_2 (at 4 nm, $e^{-2} \approx 0.1$), and XPS Si 2p measurements probe the Si energy levels in the top ~4 nm of the Si.

To utilize the Kraut method, the energy offset between a Si or Ti core level and *E* V of separate Si or TiO_2 layers was established. Following interface formation, measured energy differences between the chosen Si and Ti core levels were used to yield the heterojunction ΔE_V (and ΔE_C since the band gaps are known) band offsets. As shown, the measured band offsets are determined by the difference between the TiO_2 energy levels in the vicinity of the free TiO_2 surface, and the Si energy levels near the interface. Consequently, the measured band offsets are the sum of the abrupt band offsets right at the TiO_2/Si interface and band bending in the TiO_2 from the near surface to the interface. Henceforth, the band offsets will be referred to explicitly and implicitly as device-relevant band offsets. The Ti2p core level was chosen for its larger photoionization cross-section (at the soft X-ray photon energy used, 1486.7 eV) as compared to the other Ti core levels. The Si 2p and 2s core levels have the largest photoionization cross-sections, which are comparable in magnitude. In order to determine *E* Si $2p_{3/2}$ (Si) – E_V(Si), and given the unknown density of states at the valence band top of the H-passivated Si surface, initially H-passivated n^+-Si (10^{18} cm^{-3}) and p^+-Si (10^{18} cm^{-3}) samples were argon-ion sputtered in high vacuum to induce a large density of surface states, which are known to pin the Fermi level at ~0.4

eV above E_V (Si) regardless of the doping type. Confirming this point, the same energy position of 99.38 eV below E_F was found for the Si $2p_{3/2}$ peak in both cases (n^+- and p^+-), yielding a value for $E_{Si2p3/2}(Si) - E_V(Si)$ of 98.95 eV, comparable to values reported by others [S. Hu, M. R. Shaner, J. A. Beardslee, M. Lichterman, B. S. Brunschwig, N. S. Lewis, Science, vol. 344, 1005 (2014)]. For the $E_{Ti2p3/2}(TiO_2) - E_V(TiO_2)$ offset, the energy position of $E_V(TiO_2)$ with respect to E_F, obtained from UPS Helium II measurements, was subtracted from E Ti2p3/2 (TiO_2) with respect to E_F , obtained from XPS measurements. The resulting E Ti2p3/2 (TiO_2) – E_V (TiO_2) offset ranged from 455.38 to 455.77 eV.

The average of the offset values — 455.58 eV — was used. The density of charged surface states on the H-Si surface only, prior to TiO_2 deposition, is estimated from the Si band bending. Measurements of $E_{Si2p3/2}$ (Si) for H-n^+-Si and H-p^+-Si yield values of 99.73 and 99.15 eV, respectively. Band bending in Si is obtained from the energy difference between E_V (Si) at the interface and in the bulk. The interface position with respect to E_F is deduced from the Si2p core level energy. The bulk position is calculated by taking the lower bound of the resistivity range, obtaining the equivalent doping concentration, and calculating the energy position of E_F using the Maxwell–Boltzmann approximation. The bands bend ~0.2 eV down for H-p^+-Si, and ~0.3 eV up for H-n^+-Si (Figure 19).

To estimate the surface state/defect density, we calculate the total charge contained in the Si depletion region using the standard width W of the depletion region. Taking H-n^+-Si as an example, and using values of $\Delta V \approx 0.3$V, $N_D \approx 1 \times 10^{18}$ cm^{-3}, the depletion region is estimated to be ~20 nm wide. The silicon surface state density, obtained by multiplying the bulk doping concentration by the depletion region width, is estimated to be ~2×10^{12} states cm^{-2}. H-Si prepared with simple wet chemical processing in ambient conditions yields therefore reasonably low surface

state densities, with ~1 defect per 350 atoms at the surface. XPS measurements were performed on a series of TiO_2/Si heterojunctions, for Si n- and p-doping ranging in concentration from 10^{16} to 10^{19} cm^{-3}. Using the Kraut method described above, these measurements yield the complete energy diagrams of these heterojunctions as shown in Figure 19**.** Measured and derived values are summarized in Table 1 of [G. Man, et al., Advanced Materials Interfaces, vol. 3, (2016)].

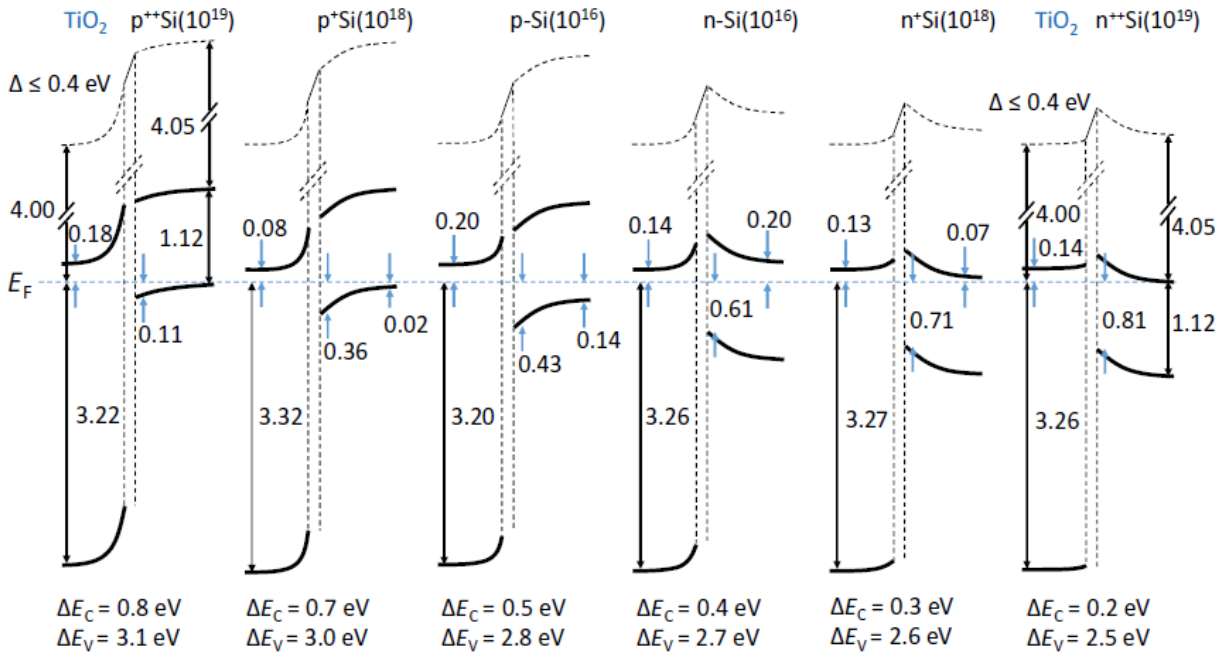

Figure 19. Heterojunction interface dipole and device-relevant band offsets of as-deposited TiO_2 on a variety of n-Si and p-Si. The vacuum level is shown as a dashed line to visually aid the reader, as it does not actually exist in the bulk of a solid.

The key result is the shift of the Fermi level at the Si surface, showing the absence of Fermi level pinning, as the silicon doping evolves progressively from p^{++} to n^{++} (Figure 19). The TiO_2 energy levels shift monotonically with respect to those of Si, as exemplified by the heterojunction valence band offset, which changes from 3.11 eV for TiO_2 /p^{++}-Si to 2.45 eV for TiO_2 /n^{++}-Si. Recall that the measured ΔE_V is the energy difference between E_V (TiO_2) at the free surface of the TiO_2 and E_V(Si) at the interface. Irrespective of the bulk Si doping type and concentration, the

Fermi level in the band gap of TiO_2 is always positioned at ~0.1–0.2 eV below $E_C(TiO_2)$, confirming the n-type character of as-deposited TiO_2. There is no observable asymmetry in any of the Ti 2p peaks (comparing the Ti $2p_{3/2}$ peak spectra and curve fit), which indicates that the energy levels are flat in the ~4 nm of TiO_2 near the free surface. There are three implications associated with this finding. First, there is a negligible surface state density at the free surface of the TiO_2, otherwise band bending would be present. Second, if a depletion region originating from charge transfer to/from the Si or interface states is present in the 10–15 nm thick TiO_2 films, its width is ~10 nm. The absence of Fermi level pinning at the c-Si interface results from the chemical/hydrogen passivation of silicon, which remains largely intact throughout the TiO_2 deposition process, and the absence of intrinsic interface-induced gap states. These measurements show that Fermi level equilibration is the primary mechanism behind the TiO_2 /Si band alignment. Third, based on the discontinuity in electric field at the interface, negative charge may exist in the TiO_2 near the interface.

III.C. Task Summary

- As the Si doping concentration and type are progressively changed from p^{++} to n^{++}, the silicon energy band position at the TiO_2 /Si interface changes by ~0.7 eV according to photoemission spectroscopy measurements, unequivocally demonstrating that the Fermi level at the interface is not pinned.
- The TiO_2 has a Fermi level near its conduction band – it is n-type.
- Consequently, Fermi level equilibration between the naturally n-doped oxide and Si is found to be the driving mechanism behind the heterojunction energy level alignment.

- The large band gap and deep valence band edge of TiO_2 insures the formation of an efficient hole-blocking carrier-selective interlayer at the electron-collection contact of the Si solar cell, and that gap states at the interface may play a role in the remaining current mechanisms.
- The surface of both n-type and p-type Si is somewhat depleted, with a potential a few tenths of an eV from that in the bulk. This is inconsistent with both field passivation, where accumulation or inversion would be expected, and chemical passivation, where any depletion would not be expected to yield the very low surface recombination velocities observed in the Task 3 Section of this report.
- The band diagrams show an energy peak near the TiO_2 surface, suggesting negative charge may exist near the TiO_2 surface.

IV. Task 3: Interface Defects and Silicon/Metal Oxide Interface Recombination

Results in this section are published in large part in

J. Jhaveri, S. Avasthi, G. Man, W. E. McClain, K. Nagamatsu, A. Kahn, J. Schwartz, and J. C. Sturm, "Hole-blocking crystalline-silicon/titanium-oxide heterojunction with very low interface recombination velocity," in 2013 IEEE 39th Photovoltaic Specialists Conference (PVSC), ed, 2013, pp. 3292-3296. doi: 10.1109/PVSC.2013.6745154

J. Jhaveri, S. Avasthi, K. Nagamatsu, and J. C. Sturm, "Stable low-recombination n-Si/ TiO_2 Hole-blocking interface and its effect on silicon heterojunction photovoltaics," in 2014 IEEE 40th Photovoltaic Specialist Conference (PVSC), ed, 2014, pp. 1525-1528. doi: 10.1109/PVSC.2014.6925206

IV.A. Approach and Method

A key motivation for our investigation of the n-Si/ TiO_2 interface is that it reduces the current of minority carrier holes compared to that at a n-Si/metal interface. However defects at the n-Si/ TiO_2 interface can themselves facilitate recombination of minority carriers, which can

negate the hole-blocking properties of the n-Si/TiO_2 interface. The recombination rate (R_{int}) is given by:

$$R_{\text{int}} = p_s \cdot s \qquad (2)$$

where p_s is the surface minority carrier density assuming no band bending. The interface recombination velocity (cm/s) is represented by s. The recombination velocity is directly proportional to the number of interface defects as shown by

$$s = N_{it} v_{th} \sigma_p \qquad (3)$$

Where N_{it} is the interface defect density, v_{th} is the thermal velocity of holes and σ_p is the capture cross section for holes. The interface recombination velocity can be calculated by measuring the effective lifetime as given by the following

$$\frac{1}{\tau_{eff}} = \frac{1}{\tau_{bulk}} + \frac{s_{front}}{W} + \frac{s_{back}}{W} \qquad (4)$$

where τ_{eff} is the actual measured effective lifetime of the minority carriers, τ_{bulk} is the lifetime associated with the bulk, s_{front} and s_{back} are the recombination velocities associated with the front and back interfaces and W is the width of the substrate. We assume the minority carrier diffusion length is much longer than the substrate width.

Lifetimes were measured using the Quasi-steady State Photoconductance Decay (QSSPCD) with 300-um 2 x 10^{15}/cm^3 n-type silicon FZ wafers, with bulk lifetimes larger than 1 ms. First, a high-quality thermal oxide was grown on both Si wafer surfaces at 1050 °C to passivate the surface. From the measured effective lifetime, a worst-case value (assuming an infinite τ_{bulk} and no Auger recombination at low excitation densities) of s of 20 cm/s was extracted for both top and bottom Si/SiO_2 interfaces at an excess minority carrier density of 5 x 10^{15} cm^{-3}. Then the oxide

on the top was etched off and a native oxide was allowed to grow on the top surface. The effective lifetime was measured again. As expected from the high number of interface defects on the top surface, a low effective lifetime of 10 us was measured. Next, after native oxide removal, TiO_2 was deposited at room temperature and the lifetime was measured once more. The effective lifetime improved to 40 us. Assuming the bulk lifetime and the back side Si/SiO_2 interface did not change, an s of 1900 cm/s was extracted for the as-deposited Si/TiO_2 interface.

After annealing at 250°C for 2 minutes in N_2, the effective lifetime increased to 340 us at a minority carrier density of 5 x $l0^{15}$ cm^{-3} (Figure 20), which corresponds to an s value of 70 cm/s for n-Si/TiO_2. There was little dependence on excitation density, so that effects like surface charging (probably) or high level injection (more certainly) can be ruled out.

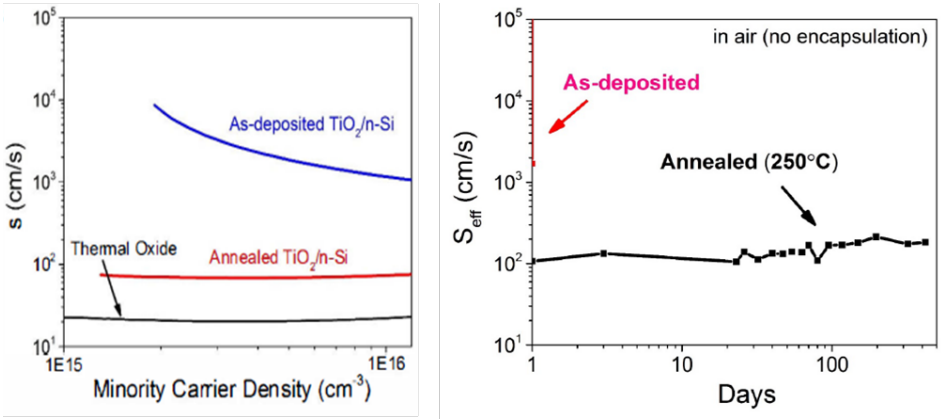

Figure 20. n-Si/ TiO_2 recombination velocity versus minority carrier density, and stability of s vs days in air for over 1 year, both as-deposited and after annealing at density of 5 x $l0^{15}$ cm^{-2}.

IV.B. Stability and Annealing

For practical applications, stability of the interface is critical. Therefore, we exposed samples to air at room temperature. The interface recombination velocity increased to 100-200 cm/s after a few days and remained near this value for over 400 days. Assuming σ_p is 10^{-16} cm^2, an s of 200 cm/s implies a defect density of ~ 2 x 10^{11} cm^{-2} , i.e. only 1 in 10,000 Si atoms is

unpassivated. For reference, the best thermal SiO_2 passivated surfaces have a defect density of ~ 2 x 10^{11} cm^{-2}. We attribute this excellent surface passivation in part to the formation of bridging Si-O-Ti bonds between the Si and TiO_2 networks (Task 1), but the results are not consistent with the band bending observed in Task 2, an issue still unresolved.

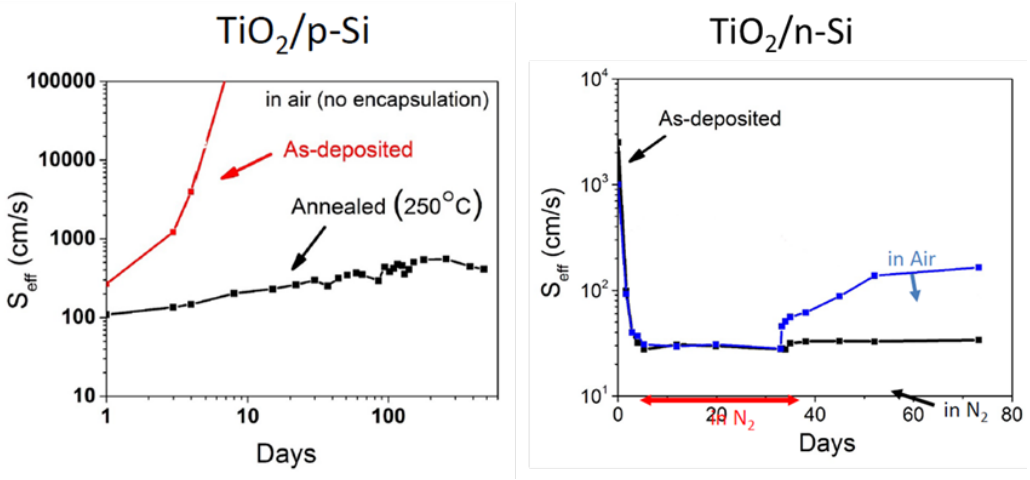

Figure 21. p-Si/ TiO_2 recombination velocity s vs. days in air, both as-deposited and after annealing, and stability of s on n-Si/ TiO_2 in both N2 and air for "room temperature annealing."

Similar behavior (rapid degradation as-deposited, and reasonably stable after 250 ^oC annealing) was also found for TiO_2 on p-type silicon (Figure 21), although after 1 year the effective recombination velocity rose to ~400 cm/s, vs. 100-200 cm/s on n-type substrates. The increase may be due to degradation of the p-S/SiO_2 interface in the test structure on the backside, as that has been reported in the literature, instead of the degradation at p-Si/ TiO_2.

"Room-temperature" Annealing

We also report on "room-temperature annealing", where instead of heating to elevated temperature, a sample was simply left inside a glove box with nitrogen ambient. Within ~2-3 days, the effective interface recombination velocity of n-Si/ TiO_2 dropped to only 30 cm/s! This is within a factor of ~ten of the best passivation ever reported on silicon, and sufficient for highly

efficient solar cells. However, after moving the samples to air, the effective s rose to the same 100-200 cm/s range seen after long term air exposure for samples annealed at 250 ^{o}C in N_2.

None of the annealing conditions (250 ^{o}C or room-temperature in N_2) substantially changed the band-alignments as shown in Figure 11.

IV.C. Task Summary

This results suggest

- The Si/TiO_2 interface can be prepared with extremely high quality (s in the 30 cm/s range or better).
- It degrades slowly in air to the ~100-200 (n-type) or ~400 cm/s (p-type) range, perhaps because of some interaction with air.
- That both n-type and p-type surfaces can be passivated suggests that a true “chemical passivation” is occurring (reduction of interface defects), rather than “field passivation” alone (a large surface charge causing accumulation or inversion to reduce – leading to a large denominator in the Shockley-Read-Hall equation for recombination rate).
- Neither option (chemical or field passivation) is 100% consistent with the observed interface band structure (Task 2), which suggests some negative charge near the Si/ TiO_2 surface, and also depletion of the silicon for both n-Si and p-Si.

V. Task 4: Electrical device barrier probes and Integrated PV device application

V.A. TiO_2/n-Si as a minority-carrier (hole)-blocking and electron-transparent contact

Results in this section are largely published in:

K. A. Nagamatsu, S. Avasthi, G. Sahasrabudhe, G. Man, J. Jhaveri, A. H. Berg, J. Schwartz, A. Kahn, S. Wagner, and J. C. Sturm, "Titanium dioxide/silicon hole-blocking selective contact to enable double-heterojunction crystalline silicon-based solar cell," Applied Physics Letters, vol. 106, (2015). doi: 10.1063/1.4916540

S. Avasthi, K. A. Nagamatsu, J. Jhaveri, W. E. McClain, G. Man, A. Kahn, J. Schwartz, S. Wagner, and J. C. Sturm, "Double-heterojunction crystalline silicon solar cell fabricated at 250 ^{o}C with 12.9% efficiency," in 2014 IEEE 40th Photovoltaic Specialist Conference (PVSC), 2014, pp. 949-952. doi: 10.1109/PVSC.2015.7356054

J. Jhaveri, K. A. Nagamatsu, A. H. Berg, G. Man, G. Sahasrabudhe, S. Wagner, J. Schwartz, A. Kahn, and J. C. Sturm, "Double-heterojunction crystalline silicon solar cell with electron selective TiO_2 cathode contact fabricated at 100 ^{o}C with open-circuit voltage of 640 mV," in 2015 IEEE 42nd Photovoltaic Specialist Conference, 2015. doi: 10.1109/PVSC.2015.7356054

K. Nagamatsu, Crystalline Silicon Photovoltaics via Low-Temperature TiO_2/Si and PEDOT/Si Heterojunctions, Ph.D. Thesis, Princeton University, January, 2016. (http://www.princeton.edu/sturm/publications/phd-theses/)

In this section we discuss the realization of the PV device structure in Figure 1(b), repeated in Figure 22, where PEDOT/Si is used to replace the p^+-n Si junction and n-Si/TiO_2 is used to replace the n/n^+ back-side field junction. We start with some theory and modelling of the function of the hole-blocking layer.

Modelling of Effect of Hole Blocking Layer on interface Recombination at Si/TiO_2 neutral contact.

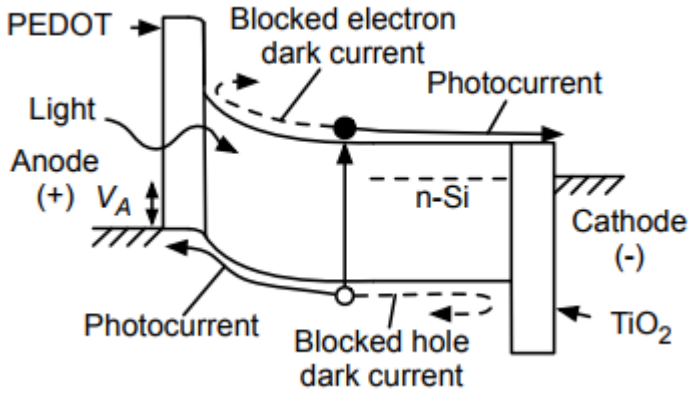

Figure 22. Device structure under study in this section, with focus on the hole-blocking properties of the TiO_2 layer at the n-Si neutral contact (cathode). Repeated from Figure 1 (b).

The device under study in this section has a band diagram shown in Figure 22. An Al/PEDOT/n-Si interface functions as the minority carrier injector (and provides the electric field for the photocurrent collector). The TiO_2 layer at the cathode side (the neutral contact) has the function of blocking minority carrier holes from reaching the cathode metal, thus reducing the hole current and reducing dark current. As noted in the introduction, a critical factor is the recombination of holes at the n-Si/TiO_2 interface. Figure 23 shows the expected hole profiles under conditions of both (a) a fixed voltage applied to the device (which fixes the minority carrier hole density on the anode size of the neutral substrate (the injecting side), or (b) a fixed hole current, corresponding to a constant slope of the hole density assuming no bulk recombination in high lifetime substrates. If the hole blocker were perfect, there would be no hole current, and the hole profiles would be flat with zero slope. However, recombination at the Si/TiO_2 interface will result in hole current and thus the profiles having a slope.

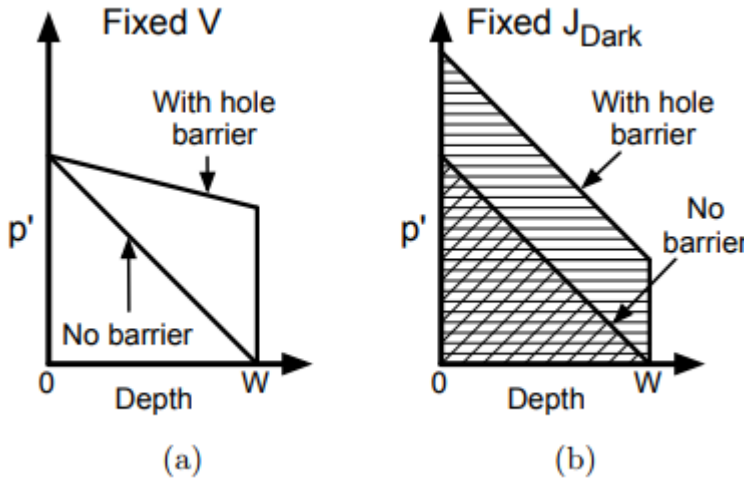

Figure 23. Excess minority carrier hole concentration in the quasi-neutral region of silicon substrate with (a) fixed forward bias voltage and (b) fixed forward bias current for a hole-blocking layer at a neutral contact to n-type Si as in (b). Compared are the hole profiles of a device with and without a hole-blocker at the cathode. The cross-hatched areas in (b) indicate the amount of stored charge due to the injected minority carriers in the quasi-neutral region of the devices.

We define the "blocking factor" BF as the factor of reduction in the hole current caused by the TiO_2 layer for a fixed applied voltage. We have shown that the blocking factor is

$$BF = 1 + \frac{D_{p,N}}{W \cdot s_{Si/TiO2}} \qquad (5)$$

where $D_{p,N}$ is the hole diffusion constant in the n-type substrate, W is the substrate thickness, and $s_{Si/TiO2}$ is the Si/TiO_2 interface recombination velocity [K. A. Nagamatsu et al, "Titanium dioxide/silicon hole-blocking selective contact to enable double-heterojunction crystalline silicon-based solar cell," Applied Physics Letters, vol. 106, (2015)]. Note as the interface recombination velocity increases, the blocking factor decreases as intuitively expected. Also note that in Si-based devices, where a thick substrate is required for the absorbing region (large *W*), a low s is important. In organic devices with thin layers, *s* may be less important, although *D* correspondingly is small as well.

When the hole current dominates the dark current (e.g. a near-unity minority carrier injection efficiency at the anode interface), the dark current will decrease by this amount. As an example, when the substrate thickness is 300 um, diffusion constant is 11 cm^2/s, and the interface recombination velocity is 200 cm/s, the expected blocking factor is ~2.8, corresponding to nearly a 3X reduction in dark current. Under low-level injection conditions, this blocking factor would correspond to a larger voltage being needed to yield the same hole current, with an increase in applied voltage ΔV_{pn} . This would directly translate into an increased open-circuit voltage ΔV_{OC} of the same amount.

$$\Delta V_{pn} = \Delta V_{OC} = {}^{kT}/_{q} \cdot \ln(BF) \quad (6)$$

Finally, we note, that without any backside field or barrier, the dark current due to holes in low-level injection would be (the usual "short-base" equation)

$$J_{dark} = \frac{qn_i^2 D_{p,N}}{WN_D}(e^{\frac{qV}{kT}} - 1) \quad (7).$$

With the backside hole barrier, by definition of the blocking factor, this would be reduced to

$$J_{dark,with\ hole\ barrier} = \frac{1}{1+\frac{D_{p,N}}{W \cdot s_{Si/TiO2}}} \quad \frac{qn_i^2 D_{p,N}}{WN_D} \ (e^{\frac{qV}{kT}} - 1) \quad (8)$$

Device Fabrication

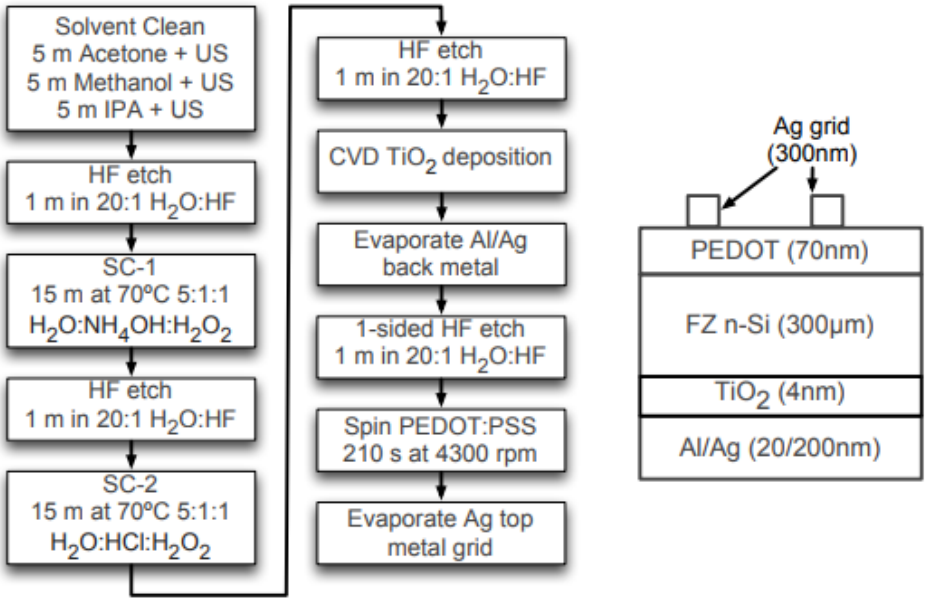

Figure 24**.** Fabrication process and structure of double-heterostructure Si-based solar cell, consisting of PEDOT/n-Si/TiO_2 (PST). For control devices the TiO_2 was omitted.

The fabrication process of the PEDOT/Si/TiO_2 Solar Cell is shown in Figure 24. For the double-sided heterojunction solar cells, in order to reduce losses due to bulk recombination, float-zone wafers with high bulk-lifetime were used, which had a phosphorus doping concentration of 10^{15} cm^{-3}. These wafers had a thickness of 300 µm and were double-side polished. Immediately following the final HF dip of the cleaning procedure, the 16 mm × 16 mm silicon samples are placed into the TiO_2 deposition chamber. The thin films are deposited using the cycled growth method described in Section II. For the devices fabricated and discussed within this chapter a standard deposition of 3 cycles was used (unless specified otherwise). The samples received a "room-temperature" anneal in a nitrogen glove box for ~2 days before metallization. (Room-

temperature annealing yielded better device results than the 250^{o}C anneal also mentioned in Task 3). Aluminum and silver metal were evaporated to form the contact on the cathode side of the device.

The TiO_2 is deposited on both sides (anode and cathode) of the silicon samples during the low-temperature CVD process during a standard deposition. The TiO_2 on the anode side of the sample is etched away with the use of a PDMS mold, which allows the application of 20:1 H_2O:HF acid to only one side of a 16 mm×16 mm. This allows the TiO_2 and metallization on the cathode side to remain while the anode side is etched. Immediately following the HF acid etch, the sample is rinsed with deionized water, blown dry using nitrogen, and the anode side of the device is spin-coated with PEDOT:PSS at 4300 rpm, to give a thickness of ~70 nm. After PEDOT:PSS coating the samples are then placed under vacuum for thermal evaporation of the front side metal grid. Three grid designs were used that covered 5.4 %, 9.7 %, and 16.2 % of the top surface area of the device.

We now experimentally demonstrate the performance of TiO_2 as an effective hole blocker in photovoltaic devices. To that end, the double-sided heterojunction device (PEDOT/Si/TiO_2) is compared to a single-sided heterojunction device (PEDOT/Si).

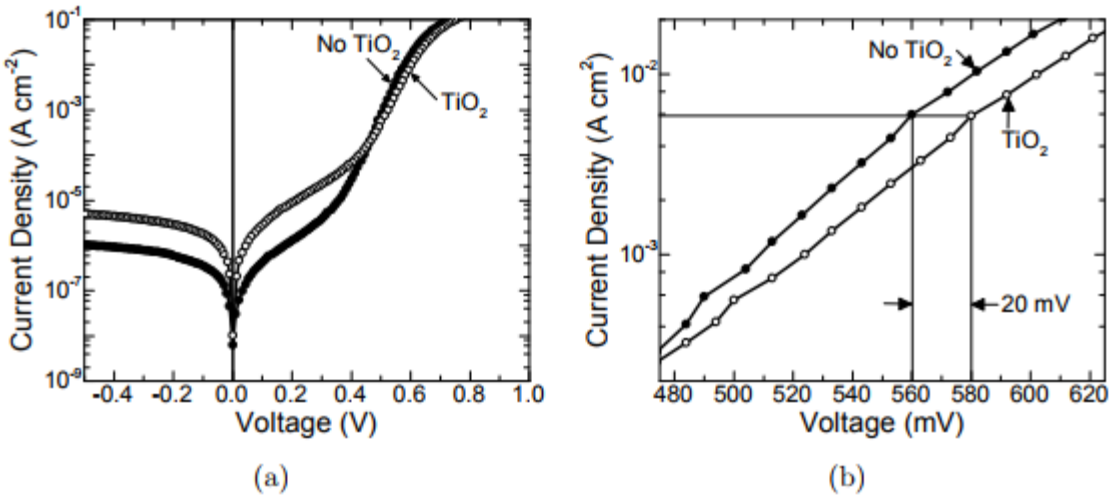

Figure 25. (a) Current-density vs voltage characteristics of single-sided and PST solar cell in the dark. (b) Close-up of ideal (n=1) exponential region showing ~20 mV shift to higher voltage for same current caused by TiO_2 hole blocker.

Dark Current-Voltage Characteristics

The current density-voltage (J-V) characteristics of a PEDOT/Si and PEDOT/Si/TiO_2 (PST) device as measured in the dark are presented in Figure 25(a). Both devices show some non-ideal (n>1) current in reverse and low forward bias (<0.4 V). The source of this non-ideal current may be caused by the differences in the fabrication process needed to make the PEDOT/Si/TiO_2 (abbreviated as PST below) devices, compared to the PEDOT/Si devices without TiO_2. However, in the ideal portion of the log(J)-V characteristics where n≈1, most significantly, the current in the double-sided device is reduced substantially compared to the single-sided one. A closer view of the ideal exponential portion of the log(J)-V curves in forward bias is shown in Figure 25(b). Here it becomes easier to quantify the amount of current reduction. For a fixed bias voltage, the hole-blocking layer causes a 1.8-fold reduction in the dark current-density that flows in the double-sided device compared to the single-sided device. Equivalently, to reach the same current-density a 20 mV greater bias voltage is required for the double-sided heterojunction device.

Using Equation (5) and values of hole diffusion constant $D_{p,N}$ = 11 cm/ sec and wafer thickness W = 300 μm, a BF blocking factor of 1.8 gives an estimated surface recombination velocity $s_{Si/TiO2}$ of ~460 cm/ sec. The blocking factor taken from the dark J-V is one method for estimating the SRV of the Si/TiO_2 interface in an actual device. This is important, as the TiO_2 films within the PV devices described here receive metal, whereas those used to measure SRV via the Quasi-Steady-State Photoconductance Decay (QSSPCD) method presented in Task 3 (Surface Passivation) do not. Because the TiO_2 layers are so thin (~3-4 nm), any interaction of the metal with the TiO_2 could lead to metal penetrating through the TiO_2, or further reducing its thickness to allow hole tunneling through the TiO_2. Therefore several measurements of the PST solar cell are employed to make estimates of the SRV of the Si/TiO_2 interface.

Illuminated Current-Voltage Characteristics: Increase in V_{OC} and I_{SC}

The J-V characteristics of the single-sided and double-sided devices under AM1.5G illumination are shown in Figure 26 and the solar cell performance parameters are shown in Figure 27. AM1.5G measurements were made using an OAI systems AAA Tri-sol solar simulator, and a 4 mm × 4 mm aperture was used to ensure accurate estimation of photocurrent. Solar simulator output was measured using a silicon reference cell (PV Measurements Inc.) that was calibrated using Newport Corporations PV Cell Lab. All calculations use total device area (4 mm × 4 mm), including the metalized grid, which covered about 16% of the device surface. Note that both the device with and without TiO2 are “well-behaved.” No excessive series resistance or parasitic barriers are observed. For example, a parasitic conduction band barrier at the Si/TiO_2 interface would led to a dependence of photocurrent on the device voltage. This is consistent with tests of the I-V characteristics of Al/TiO2/n-Si, in which purely Ohmic behavior at room temperature was

observed [S. Avasthi et al, "Hole-blocking titanium-oxide/silicon heterojunction and its application to photovoltaics" Applied Physics Letters, vol. 102, (2013)].

The double-sided device (with TiO_2) shown exhibits a significant improvement over the single-sided device of over 30 mV in V_{OC}. This is further evidence that the dark current is reduced at the Si/TiO_2 interface due to the hole-blocker, as this increase in V_{OC} agrees to first order with the shift observed in the dark current characteristics of 20 mV. Parameters are summarized in Figure 27.

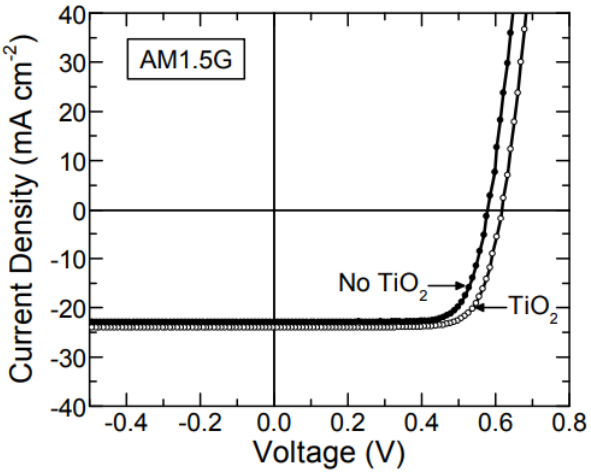

Figure 26. Current-voltage characteristic of a PEDOT/Si solar cell with and without TiO_2 hole blocker under AM1.5G illumination.

Device	V_{OC}(mV)	J_{SC}(mA cm^{-2})	FF(%)	η(%)
No TiO_2	583	22.9	77.1	10.3
With TiO_2	614	24	76.2	11.2
Δ	+31	+1.1	-0.9	+0.9

Figure 27. Performance comparison of PEDOT/Si and PEDOT/Si/TiO_2 solar cells, with substrates held at ~25 ºC.

The measured improvement in open-circuit voltage ΔV_{OC} can also provide an estimate of the SRV at the Si/TiO_2 interface. Using the observed open-circuit voltages of the devices in Figure 27 the SRV at the Si/TiO_2 interface can be estimated to be ~170 cm/s. However, this contrasts to the value estimated from dark J-V measurements of ~460 cm/ sec for the Si/TiO_2 interface. It is useful to also consider the average values of V_{OC} of the devices. The average and standard deviation of V_{OC} for eighteen PEDOT/Si devices and eighteen PST devices are (588 ± 4) mV and (613 ± 5) mV, respectively, which provides an average value of ΔV_{OC} of (25 ± 7) mV. This leads to an estimate of SRV between 150 to 460 cm/s, a range which is closer to the value estimated from the dark J-V measurement.

The hole-blocking TiO_2 layer also consistently was observed to improve the short-circuit current density in the PST device. The single-sided device exhibits a short-circuit current of 22.9 mA cm^{-2}, while the double-sided device achieved a J_{SC} of 24.0 mA cm^{-2} , an increase of 1.1 mA cm^{-2}. On average (for 16% coverage of the top metal grid), the J_{SC} of single-sided devices was (22.8 ± 0.5) mA cm^{-2} and of double-sided devices was (23.6 ± 0.4) mA cm^{-2}, a difference of 0.8 mA cm^{-2}. The increase in short-circuit current density can be attributed to reduced recombination of photo-generated holes at the rear interface of the solar cell due to the TiO_2 hole blocker, which will be discussed after the following Power Efficiency and Optical Loss Section.

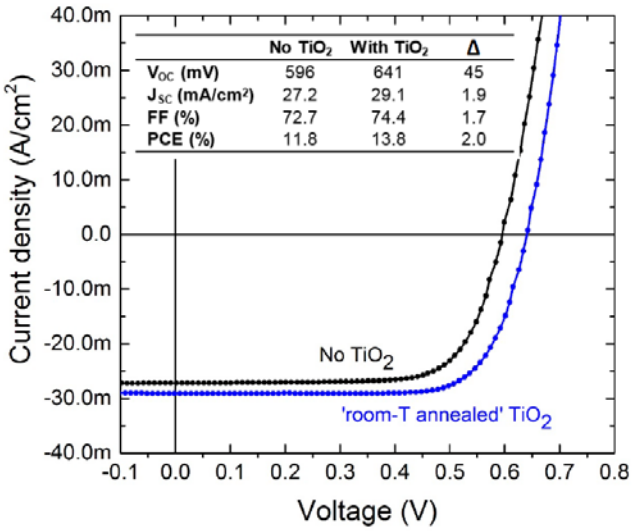

Figure 28. Best device results in terms of open circuit voltage increase and power conversion efficiency. The increase in V_{OC} corresponds to an interface recombination velocity at Si/TiO_2 of ~ 80 cm/s.

Figure 28 shows a best device from a different process run, with similar fabrication to the devices analyzed above. In this device an increase in V_{OC} of 45 mV was observed. Using Eq'ns. (5) and (6), this corresponds to a blocking factor BF of 5.5, and an effective interface recombination velocity at the back interface of ~80 cm/s. This is similar to the numbers measured with pulsed photoconductivity in surface passivation experiments. We attribute the increase compared to the earlier run to a higher quality front PEDOT/Si interface, for reasons unknown. Excessive recombination at that interface leads to an excessive electron current at the PEDOT/Si junction, so that reducing hole current by a barrier at Si/TiO_2 has less effect.

The 29 mA/cm^2 short circuit current was limited almost entirely by absorption in the PEDOT and surface reflection, with metal coverage (16%) also contributing (next section). Straightforward engineering to raise the short circuit current to ~42 mA/cm^2 would raise the power efficiency to over 20%, consistent with that expected with s = 80 cm/s in Figure 3.

Overall Power Efficiency and Optical Losses

Overall, the best device (Figure 28) shows an absolute improvement of 2.0%, from 11.8% to 13.8% in power conversion efficiency over the device without any TiO_2 hole blocker. The fill factor with TiO_2 typically was the same as that without: ~75 +/- 2% showing no significant change in series resistance. Ideally the fill factor should be over 80%, and the low numbers are probably related to the PEDOT layer, since the TiO_2 has little effect.

The overall low efficiencies are due primarily due to low photocurrent, caused two effects unrelated to the TiO_2:

(i) The metal anode covered 16% of the device surface, but the entire device area was used for efficiency calculations

(ii) No AR coating or texturing was used on the top surface, and the 100-nm PEDOT layer is a significant absorber (estimated roughly at ~35% of the incident light).

This optical loss was modelled using the OPAL-2 package [K. Nagamatsu, Crystalline Silicon Photovoltaics via Low-Temperature TiO_2/Si and PEDOT/Si Heterojunctions, Ph.D. Thesis, Princeton University, January, 2016]. Figure 29 shows the reduction in photocurrent density as a function of the organic electron blocker (PEDOT:PSS) thickness. From an ideal of ~44 mA/cm^2, reflection loss and PEDOT absorption reduced the expected photocurrent to ~28 mA/cm^2. The 16% metal coverage would reduce this number to ~24 mA/cm^2, close to what was observed (23-29 mA), with the experimental variation probably due to PEDOT thickness. Thus it is clear the power efficiency results were limited by optical effects.

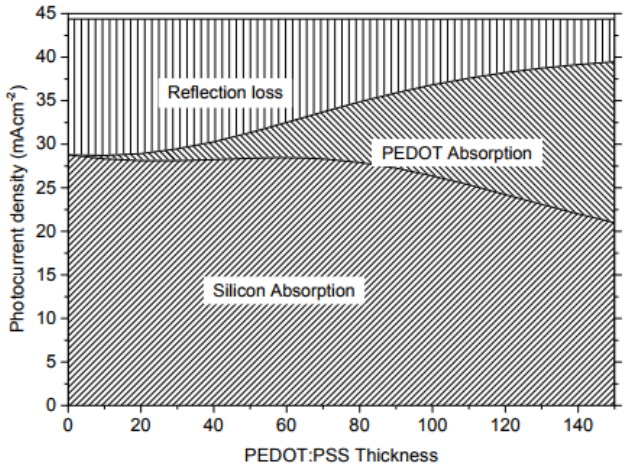

Figure 29. Short-circuit current losses from absorption and reflection as a function of PEDOT:PSS thickness for planar silicon substrate (modeled with OPAL 2).

External Quantum Efficiency

The external quantum efficiency measurements also demonstrate the ability of the TiO_2 to reduce hole recombination at the back interface. The EQE spectra for a single-sided device and double-sided device of Figure 26 are shown in Figure 30. Note at short wavelengths, where absorption is near the top of the wafer, the two devices are identical. The device with TiO_2 is superior at longer wavelengths (from 700 nm to 1050 nm), when the minority carrier holes are generated closer to the back interface, and thus are more sensitive to the back interface.

We modelled this effect numerically by using the known absorption properties of silicon, the hole continuity equation, and Eq'n. (1) for the Si/TiO_2 recombination. From the resulting carrier profiles we can calculate a quantum efficiency as a function of the interface recombination velocity. These are presented in normalized form in Figure 30(b). By "normalized EQE", we mean the improvement in quantum efficiency at a given wavelength and interface recombination velocity for a device with the TiO_2 hole blocker compared to a control device with the hole blocker.

As expected, the modelling shows that at long wavelength, the quantum efficiency is more sensitive to the back interface.

The modeling was then compared to the experimental results of the device in Figure 26 in Figure 30(a). For example, at 1050 nm, because of the hole-blocker, the EQE experimentally increased from ~29% to ~38%, an increase by a factor of 1.3. This data agrees best with the modeled curve for an interface recombination velocity of 300 cm/s. This is again consistent with the range of interface recombination velocities extracted by the decrease in dark current and increase in open-circuit voltage discussed just above for that device (150-360 cm/s), giving us confidence that this range is correct.

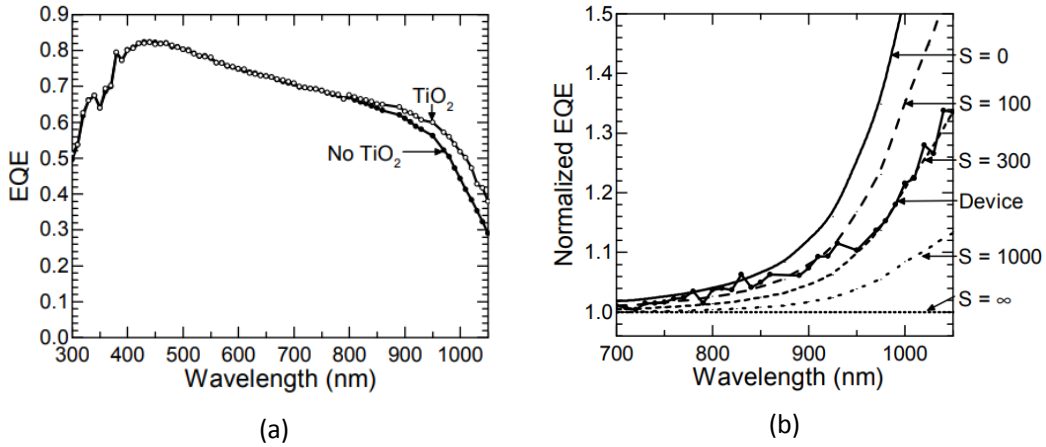

Figure 30. (a) External quantum efficiency spectra of devices with and without TiO_2 hole blocker, and (b) experimental and modelled normalized External Quantum Efficiency as a function of wavelength for different interface recombination velocities.

Using the modeled EQE vs wavelength for the device with TiO_2 (s = 300 cm/s) and the device without TiO_2 (s = infinite), and the solar spectrum, it is straightforward to integrate across the spectrum to find the expected increase in photocurrent. The calculation gives an expected increase of 1.1 mA/cm^2, which is in surprisingly exact agreement with the observed average increase of

photocurrent in the device with TiO_2 discussed above. Note the best device (Figure 28) had an increase of 2.0 mA/cm^2, consistent with its lower Si/TiO_2 interface recombination velocity of ~80 cm/s.

Stored Minority Carrier Charge

The effectiveness of the TiO_2 hole-blocking layer can also be determined by measuring the stored minority hole charge Q_{stored} in the neutral n-type silicon of the device under forward bias. For the same current in forward bias, and thus the same slope of the hole concentration profile, the double-sided device will contain a greater Q_{stored} as indicated by the crosshatched area in Figure 23(b). By switching the devices quickly to a reverse bias, and limiting the current with a resistor, one can then extract the minority carriers back out from the originally-injecting side. The length of the current in reverse bias is a measure of the stored charge to begin with, Q_{stored}, before the reverse bias. Such "reverse recovery" data is shown in Figure 31. To the best of our knowledge, this method has not previously been applied to heterojunction minority-carrier blockers as described in this work.

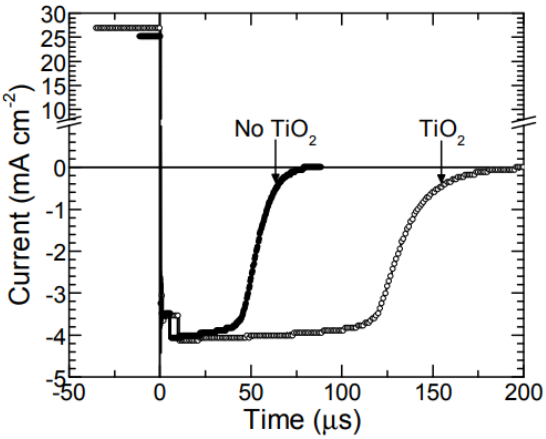

Figure 31. Reverse current as a function of time for the PST and single-sided solar cell in the reverse recovery experiment. The bias was switched at time = 0. The forward bias before switching was ~25 mA/cm^2.

The data clearly shows the increase in stored minority carrier charge caused by the hole blocker. As a first approximation, one can quantitatively compare the increase in the areas under these curves enabled by the TiO_2 to those expected from forward bias in Figure 23(b). Because the curves in Figure 23(b) depend on the rear interface recombination velocity, one can extract an effective recombination velocity from the data [K. A. Nagamatsu et al. "Titanium dioxide/silicon hole-blocking selective contact to enable double-heterojunction crystalline silicon-based solar cell," Applied Physics Letters, vol. 106, (2015)]. However, this neglects the effect of recombination at the back interface during the recovery process, and the possibility that the total current is not dominated by minority carrier injection in forward bias.

To more fully model these effects, numerical modelling of the hole currents (based on the continuity equation) was carried out as a function of time, incorporating recombination at both interfaces [A. H. Berg et al, "Extraction of Front- and Rear-Interface Recombination in Silicon Double-Heterojunction Solar Cells by Reverse Bias Transients," IEEE Transactions on Electron Devices, vol. 64, pp. 4518-4525 (2017)]. The results were formulated using a scaling method to make them applicable to a range of substrate thicknesses (L) and carrier types (different diffusion coefficients) through a scaling parameter *n*. We also found it necessary to correct for lateral current spreading, since it contributed to forward bias current but not appreciably to minority carrier collection under reverse bias. Details are in the above paper.

Typical modelling results are in Figure 32 and Figure 33. Recombination at the PEDOT/Si interface, if sufficient, would lead to a dark current which was not dominated by the hole currents, and thus the devices would be less sensitive to the hole-blocker. Thus the first step is to use single-sided devices (those with just the PEDOT electron barrier to inject minority carriers at the anode)

to find the minority carrier injection efficiency γ_{SSD} (hole current divided by total current in forward bias). This was done by using modelling and adjusting γ_{SSD} as a fitting parameter to achieve a best fit of the model to experiment, with $\gamma_{SSD} = 0.75$ giving excellent agreement (Figure 33). This means that 25% of the forward-bias current is due to recombination at the PEDOT/n-Si interface. This fact has important ramifications for the improvement of V_{OC} via lowering of the dark current. A strategy that aims only at selectively passivating the backside contact will be able to reduce the hole diffusion current but will not affect the front-interface recombination current, limiting the possible V_{OC} improvement. This means we could reduce the hole current to zero with a perfect hole blocker, but the dark current would go down only by a factor of 4 and V_{OC} up by only 35 meV. The overall improvement due to TiO_2, even with a perfect Si/TiO_2 interface, will be limited until the front side interface is improved.

The next step was to measure reverse recovery in double-sided PEDOT/n-Si/TiO_2 devices and model the data using the results of single-sided measurements to include the effects of emitter inefficiency γ_{SSD} as just described. Modelling assuming an ideal PEDOT/Si interface (as assumed in Figure 32) could not be used because of the non-ideal emitter injection ratio. Further modelling as described in the paper was performed for a variety of forward to reverse current ratios, and the forward current was also adjusted to account for the effects of current spreading. A single fitting parameter, interface recombination velocity $s(Si/TiO_2)$ was used, which yielded a value of $s(Si/TiO_2) = 330$ cm/s, a number in line with the previous measurements of that interface extracted from devices in this section.

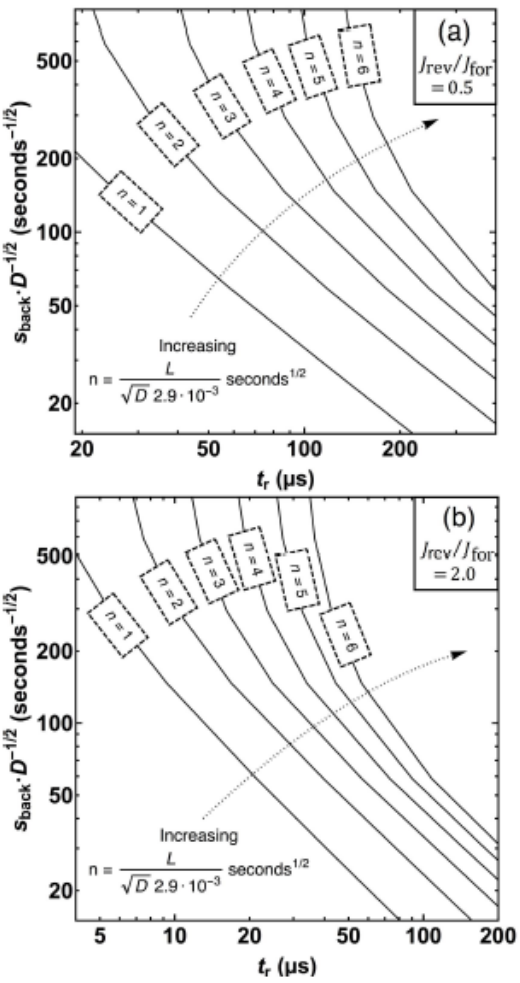

Figure 32. Backside recombination velocity $s_{Si/TiO2}$ as a function of reverse recovery time t_r in a double heterojunction device with ideal front interface, with (a) J_{rev}/J_{for} = 0.5 and (b) J_{rev}/J_{for} = 2 for a variety of $L/\sqrt{D}$ ratios.

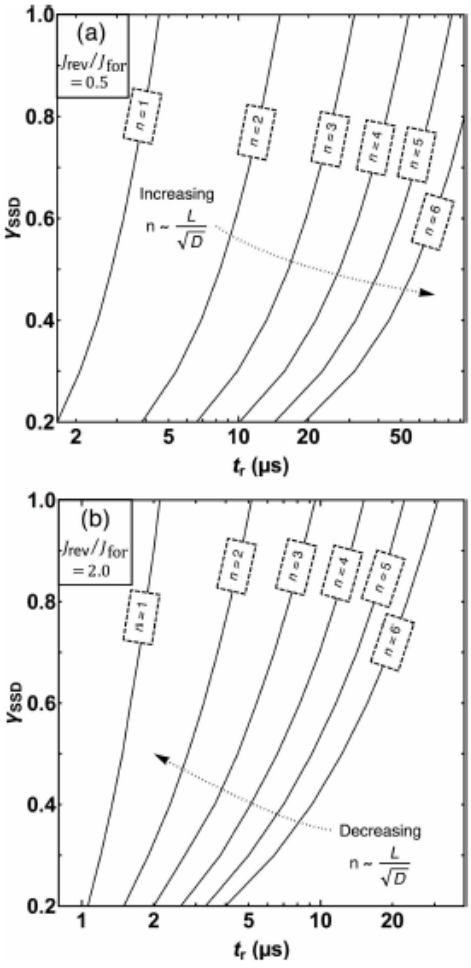

Figure 33. Injection efficiency γ_{SSD} as a function of reverse recovery time t_r in a device with PEDOT only with (a) J_{rev}/J_{for} = 0.5 and (b) J_{rev}/J_{for} = 2, where n is defined as = $L/(\sqrt{D}\ \ 2.9\cdot10^{-3})$.

Effect of Thicker TiO_2 layers and Possible Negative Charge in TiO_2

The effect of the TiO_2 layer on blocking holes in PV devices, as described extensively in this section, was found to depend on which evaporator was used to deposit the aluminum cathode. Only results from the "good" evaporator are presented in this report. Because the TiO_2 layers were so thin (~4 nm), any small interaction of the metal and the TiO_2, perhaps enabled by inadvertent heating during the evaporation process could consume some of the TiO_2, leading to a lower thickness. Thickness of < 3 nm would be expected to lead to hole tunneling through the barrier, again mitigating its effectiveness. Further, if thin layers had pin-holes, metal could penetrate in places to directly contact the silicon, again rendering the barrier ineffective.

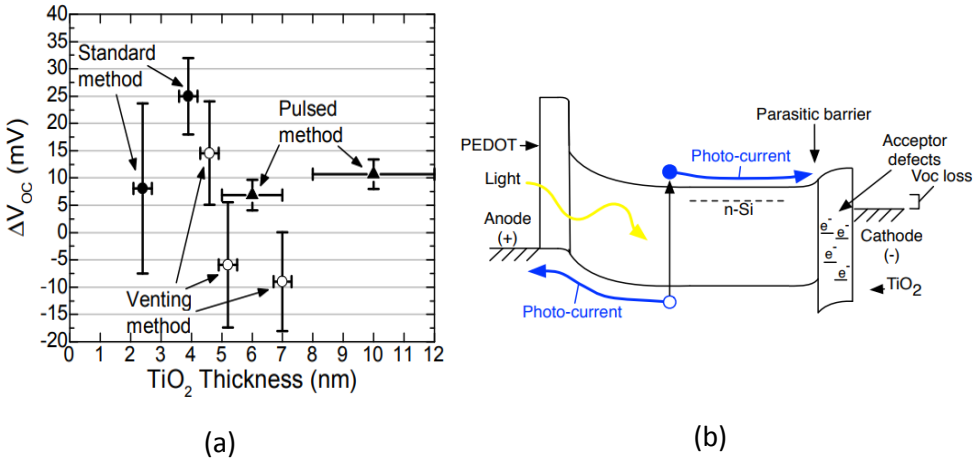

Figure 34. (a) Increase in V_{OC} vs TiO_2 thickness, using a variety of deposition modifications. (b) Schematic band diagram indicating possibility of negative charge in the TiO_2 leading to a parasitic barrier, reducing V_{OC}.

As described in the growth section of this report, we initially did not know how to grow layers beyond 4 nm, which was eventually overcome at first by venting between cycles. PV measurements to observe an increase in V_{OC}, as described above, were then repeated using the thicker TiO_2 layers. Figure 34 (a) shows that increasing the TiO_2 thickness did not increase V_{OC}. The "venting" method to achieve thicker TiO_2 resulted in a decrease in V_{OC} instead of an increase.

XPS showed a signal of unknown origin in these layers, suggesting some contamination from the venting process. By using a much larger bulb for the TiO_2 precursor with larger evaporation surface, we did finally achieve thicker layers without venting between cycles. However, this was also unsuccessful in increasing V_{OC} compared to control devices without TiO_2.

One possible explanation is that the TiO_2 layers, especially in contact with Al, have a negative charge, possibly from the transfer of electrons to acceptor states in the TiO_2 (Figure 34 (b)). This negative charge will create a barrier for the photocurrent, causing a lower voltage on the device than otherwise expected. Note that signs of negative charge in TiO_2 or at the Si/TiO_2 interface were also observed in the extensive band alignment studies presented earlier in this report.

V.B. TiO_2/p-Si as a majority-carrier (hole)-blocking and minority-carrier (electron) injecting contact

The work in this section is an updated version of what was presented at

Janam Jhaveri, Alexander H Berg, Sigurd Wagner, James C Sturm, "Measurement of TiO_2/p-Si Selective Contact Performance using a Heterojunction Bipolar Transistor with a Selective Contact," IEEE Photovoltaic Specialists Conf., Washington, DC, June 25-30, 2017.

In this section we examine the function of a TiO_2/p-Si selective contact, instead of the TiO_2/n-Si structure studied in the previous section. The contact still blocks holes and passes electrons. The goals are to examine the use of the TiO_2 as a minority carrier injection to p-type Si (replacing an n^+-p junction for PV on p-type silicon substrates), and to further understand TiO_2 models. The structure and band diagram of an experimental device is in Figure 35. In forward bias, electrons will be injected from the metal as minority carriers into the p-type silicon (process 1) as no TiO_2 electron barrier is present. Ideally, holes will be blocked by the barrier, but in reality there may be tunneling through the thin layer (process 3) or interface recombination (process 2). High lifetime FZ substrates were used.

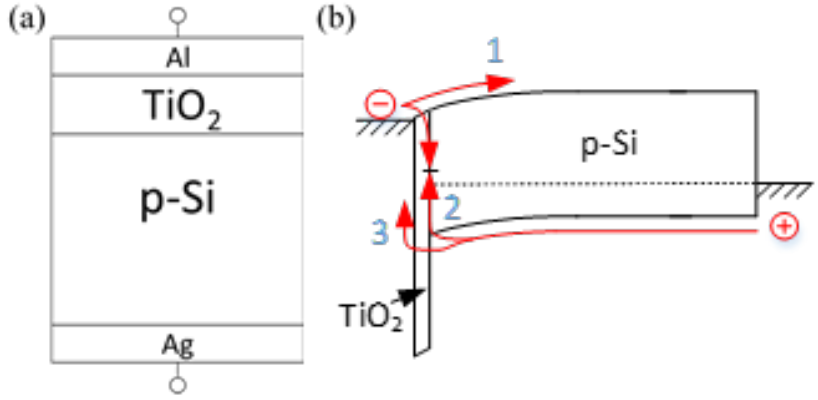

Figure 35. (a) Structure and (b) band diagram with current processes for selective contact to p-type Si.

Figure 36(a) shows the IV characteristics in the dark. The IV characteristics match those expected for a short base diode for electron injection in the substrate, with all carriers recombining at the back contact. The equation used for such current in the model in the plot was the same as (7) except for swapping n-type for p-type and holes for electrons – the standard "short-base" equation. The message is that due to the large electron current (process 1), we can't study the desired processes 2 and 3 related to the TiO_2.

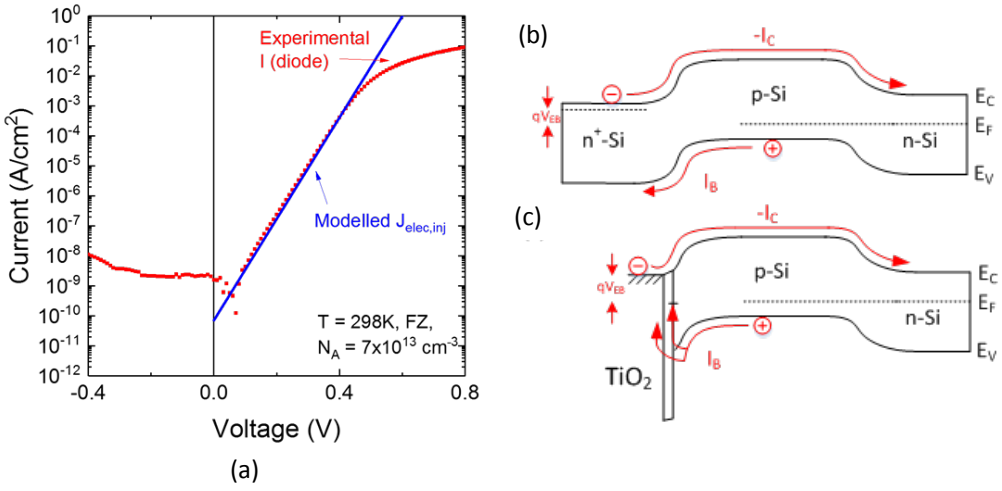

Figure 36. (a) Diode dark I-V characteristics, and band structure of (b) conventional npn bipolar transistor and (c) proposed heterojunction bipolar transistor using selective contact as the emitter.

Consider Figure 36(b) and (c), which show the band diagram of an npn bipolar transistor, and such a device (a heterojunction bipolar transistor – HBT) with the emitter replaced the by Al/TiO_2/Si selective contact, both under normal forward active mode. The injected electrons form the emitter into the p-region diffuse to form the collector current. The holes injected into the emitter, or recombining at the TiO_2/Si interface are base current. Thus with such a structure we can individually probe the electron and hole currents in a selective contact, something which before this work was impossible in a 2-terminal diode structure. Figure 37 shows the experimental structure. We started with a ~5-um p-type base layer grown epitaxially on an n-type substrate, and then deposited the TiO_2 and emitter, base, and collector contacts with appropriate masks.

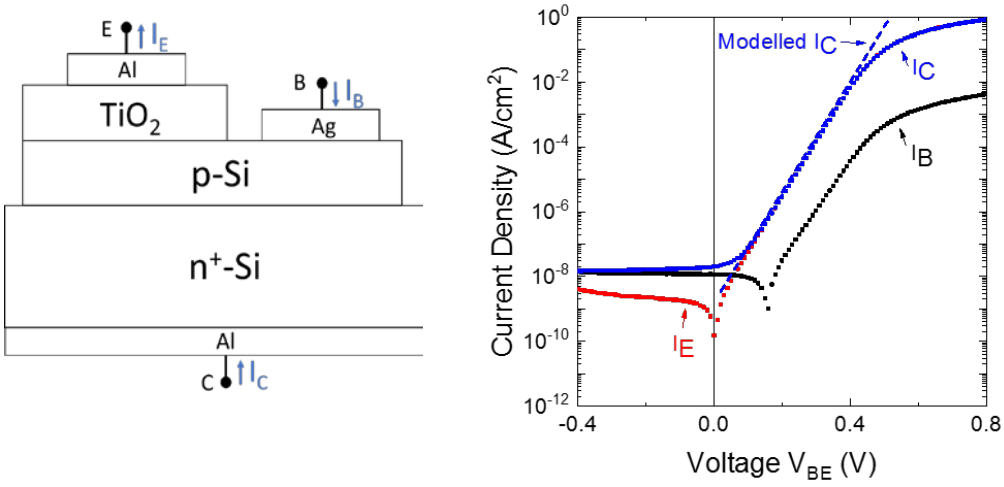

Figure 37 (a) HBT structure, and (b) Gummel plot (with V_{BC} = 0).

Figure 37(b) confirms our goal of being able to separate the electron and hole currents. The collector current, representing electrons, is much larger than the hole current; if added together in a diode we would see mainly electron current. The modelled I_C fits well with a standard bipolar collector current model. This fact and other measurements confirm the contribution of recombining electrons to the base current is negligible. The hole current (I_B) represents process (2) and (3) from Figure 35 that we want to measure.

Figure 38 shows the base current for different TiO_2 thicknesses (at a bias of 0.3V) from the HBT along with the total current in diodes as in Figure 35. There is a lot to observe:

(i) For small TiO_2 thickness, the hole current drops. This is because Process 3 (tunneling) is reduced, in both the diode and HBT base current. That the two devices are equal says hole current dominates in the diode when hole currents are large.

(ii) For ~ 4 nm TiO_2, the lowest hole current is observed. In the diode it is 10X lower than the total current, showing the power of the HBT to resolve small hole currents when there are much larger electron currents.

(iii) For thickness > 4 nm, the hole current increases again, as well as the diode total current. This is strange, but similar to what was observed in the open circuit voltages in the PV devices in Figure 34(a), where the best V_{OC} was also observed in the 4 nm range. This can't be a coincidence!

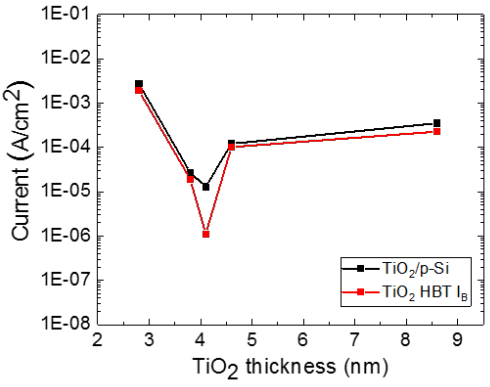

Figure 38. HBT Base current (a measurement of interface recombination) at 0.3 V, as a function of TiO_2 thickness.

Temperature dependent measurements show that as the hole current increases for thick TiO_2, the activation energy (effective barrier height) decreases from 1.01 to 0.83 to 0.78 eV. There are two things to be learned – first, the hole current is determined by an energy barrier, and second, it is decreasing with thick TiO_2. This suggests barrier formation (silicon band-banding) as a hole blocking mechanism at Si/TiO_2 interface, different from that assumed earlier in this report. That the barrier is reduced with thick TiO_2 is consistent with negative charge in the layer, as surmised in the discussion of Figure 34. These are early results, but they point the way towards a new understanding of Si/TiO_2 interfaces and hole-blocking.

V.C. Task Summary

- TiO_2 hole-blockers were demonstrated in a photovoltaic device successfully for the first time.
    - The increase in V_{OC}, due to reduced dark current, was as large as 45 mV, with V_{OC} up to 641 mV, consistent with s at Si/TiO_2 of 80 cm/s.

- The photocurrent increased by ~1 mA/cm^2 due to less recombination at the rear interface. The best I_{SC} was 29 mA/cm^2, limited entirely by absorption of light in the PEDOT and surface reflection.
- The TiO_2 had negligible effect (~2% or less) effect on fill factor.
- The best power efficiency was ~13.8%, limited largely by absorption of light in the PEDOT and surface reflection.
- With engineering to solve the absorption /reflection problem, efficiencies of ~21% are expected, with no further increase in material properties

- Effective surface recombination velocities in devices were extracted from the V_{OC} increase, the increase in long wavelength quantum efficiency, from the reduction in dark current, and from the increased stored minority charge in forward bias with fixed current, using the reverse recovery method and modelling. The effective recombination velocities were ~80-400 cm/s, perhaps 2X larger than those measured in TiO_2/Si layers by pulsed photoconductivity decay.
- The upper limit of V_{OC} is due to one or more of the following 3 effects, with the first the most important
  - Recombination at the Si/PEDOT anode interface, increasing electron current so that hole current is less significant
  - Interaction of the aluminum metallization with the TiO_2, reducing its effective thickness
  - Parasitic barriers to electrons related to the TiO_2/Si interface
- An HBT structure was presented to separately identify hole and electron currents in selective contacts for the first time.

- Using the HBTs to study hole current at the p-Si/TiO_2 interface suggests band bending in the silicon plays an important role in the hole-blocking mechanism!

VI. Project Summary

VI.A. Summary of Results

- The Si/TiO_2 interface was investigated in detail as a hole-blocker for silicon-based PV, especially to replace the n+ backside-field diffusion on cells with an n-type substrate, with a goal of reducing dark current and raise V_{OC}.
- The project introduced the concept of using TiO_2 for this purpose of an electron-selective contact. Rather than use a p+/n junction, an organic PEDOT layer was used to inject holes and collect photocurrent. Thus the final PEDOT/Si/TiO_2 structure had a maximum process temperature of 100 ^oC.
- A novel deposition process with a maximum temperature of 100 ^oC was developed (compared to ~300 ^oC for ALD), using a single precursor, with evidence of Si-O-Ti bonding across the Si-TiO_2 interface.
- A high (>> 1eV) valence band barrier and a small (<0.3 eV) conduction band barrier were measured. No evidence of any electrical conduction or photocurrent collection barriers were seen for thin (3-4 nm) TiO_2 barriers.
- Stable Si/TiO_2 interface recombination velocities of ~100 cm/s were observed after annealing at 250 ^oC or room temperature in a glove box. Velocities as low as ~30 cm/s were observed in some cases.
- The exact relationship between the interface band structure (e.g. depletion in the silicon) and low interface recombination velocities are not understood
- PV devices showed an increase in V_{OC} of up to 45 mV (to 641 mV), reflecting an Si/TiO_2 interface recombination velocity s of 80 cm/s. With a high quality minority carrier injector and good optical engineering, this is consistent with a cell efficiency of 23%.

- Our quantum efficiencies (and thus energy efficiencies) were limited by ~35-40% loss of photons due to absorption in the PEDOT layer, surface reflection, and top metal coverage. The optical issues limited I_{SC} to 29 mA/cm^2 and power efficiency to 14.1%. Without the parasitic absorption/reflection problem, a power efficiency of ~23% would be expected given the effective Si/TiO_2 recombination velocity of 80 cm/s.
- Open circuit voltages were almost certainly by recombination at the Si/PEDOT interface, causing the dark current to have a significant electron current component, so that reducing hole current with the hold blocker has limited effect. Negative charge in the TiO_2 layers may also play an effect. Addressing this issue would enable power efficiencies in the 25% range, matching those of the record a-Si/x-Si HIT double heterojunction cells.
- We have introduced a new method (HBT's) to separate hole and electron current for the study of selective contacts, and shown that the effect of TiO2 in blocking holes is at least in part due to band-banding in the silicon.

VI.B. Directions for future work and open issues

- <u>Emitter efficiency effects, alternate electron-blockers</u> The PEDOT/Si interface (replacing a p^+/Si junction) is probably limiting the ability of our TiO_2 to raise V_{OC}. Using TiO_2 as a hole-blocker on a device with a high quality p^+/Si junction will better enable us to determine the ultimate capability of the Si/TiO_2 selective contact. This also motivates further work to replace PEDOT/Si with an inorganic alternative electron blocker, such as NiO/Si, and studying its growth and interface properties.

- TiO_2 models for surface passivation and carrier blocking: We have treated the TiO_2 selective contact to n-type Si as "neutral", without any band-bending. It is now known that TiO_2 "unpins" the silicon surface Fermi level, compared to when metal is directly deposited onto Si and reacts with it to form a Schottky barrier. Thus the work function of the metal may accumulate/deplete the silicon surface underneath the TiO_2, greatly influencing the interface recombination. The interplay of silicon band-bending and interface states and how their combination affects interface recombination is a prime area for future work. This is clearly emphasized by our recent HBT work in Task 4.
- Materials Development: We are still very early in the development of TiO_2 technology on silicon, in terms of deposition methods, annealing effects, interface and bulk structure for low-temperature deposition, and so forth. Multilayers such as ultra-thin SiO_2/TiO_2 may also be attractive to separate passivation and blocking functions.

VII. Students Supported, Publications, Presentations, and Awards

VII.A. Students/ Postdocs Supported and Current Positions

1. William McClain (Ph.D. Chemistry 2015), current position: US Patent Office, Denver, CO
2. Ken Nagamatsu (Ph.D. Electrical Engineering, 2016), current position: Northrup Grumman, Baltimore, MD (semiconductor devices)
3. Girija Sahasrabudhe (Ph.D. Chemistry, 2016), current position: Post-doc, Louisiana State Univ. (efficient lighting)
4. Gabriel Man (PhD. Electrical Engineering, 2017), current position: Hunt Energy Enterprises (HEE) (solar)
5. Janam Jhaveri (Ph.D. Electrical Engineering 2018, expected)
6. Alexander Berg (Ph.D. Electrical Engineering 2019, expected)
7. Sushobhan Avasthi (Post Doc), current position: Professor at Indian Institute of Science, Bangalore, India

VII.B. Journal Publications

1. S. Avasthi, W. McClain, J. Schwartz, and J. C. Sturm, "Hole-blocking TiO_2/silicon heterojunction for silicon photovoltaics," in Device Research Conference (DRC), 2012 70th Annual, 2012, pp. 93-94. doi: 10.1109/DRC.2012.6256955
2. S. Avasthi, W. E. McClain, G. Man, A. Kahn, J. Schwartz, and J. C. Sturm, "Hole-blocking titanium-oxide/silicon heterojunction and its application to photovoltaics," Applied Physics Letters, vol. 102, (2013). doi: 10.1063/1.4803446
3. J. Jhaveri, S. Avasthi, G. Man, W. E. McClain, K. Nagamatsu, A. Kahn, J. Schwartz, and J. C. Sturm, "Hole-blocking crystalline-silicon/titanium-oxide heterojunction with very low interface recombination velocity," in 2013 IEEE 39th Photovoltaic Specialists Conference (PVSC), ed, 2013, pp. 3292-3296. doi: 10.1109/PVSC.2013.6745154
4. J. Jhaveri, S. Avasthi, K. A. Nagamatsu, and J. C. Sturm, "Wide bandgap HBT on crystalline silicon using electron-blocking PEDOT:PSS emitter," in 2013 71st Annual Device Research Conference, ed, 2013, pp. 77-78.
5. J. C. Sturm, S. Avasthi, K. Nagamatsu, J. Jhaveri, W. McClain, G. Man, A. Kahn, J. Schwartz, and S. Wagner, "Wide bandgap heterojunctions on crystalline silicon," in ULSI Process Integration 8 at the 224th Meeting of the Electrochem. Soc., also Electrochem. Soc. Trans. vol. 58 (9), pp. 97-105, 2013. vol. 58, C. Claeys, et al., Eds., ed, 2013, pp. 97-105. doi: 10.1149/05809.0097ecst
6. J. A. Spechler, K. Nagamatsu, J. C. Sturm, and C. B. Arnold, "Integrated laser processed silver nanowire transparent electrodes with organic electronic devices," in 2013 Conference on Lasers and Electro-Optics, 2013. doi: 10.1364/CLEO_SI.2013.CM1H.2
7. J. Jhaveri, S. Avasthi, K. Nagamatsu, and J. C. Sturm, "Stable low-recombination n-Si/TiO2 Hole-blocking interface and its effect on silicon heterojunction photovoltaics," in

2014 IEEE 40th Photovoltaic Specialist Conference (PVSC), ed, 2014, pp. 1525-1528. doi: 10.1109/PVSC.2014.6925206

8. J. Jhaveri, G. Sahasrabudhe, G. Man, K. Nagamatsu, S. Wagner, A. Kahn, J. Schwartz, and J. C. Sturm, "Structure of low-temperature TiO2/Si interface and impact on surface recombination for low-cost Si-based PV," presented at the 45th IEEE Semiconductor Interface Specialists Conference San Diego, CA, 2014.
9. K. A. Nagamatsu, S. Avasthi, J. Jhaveri, and J. C. Sturm, "A 12% efficient silicon/PEDOT:PSS heterojunction solar cell fabricated at < 100 ^{o}C," IEEE Journal of Photovoltaics, vol. 4, pp. 260-264 (2014). doi: 10.1109/jphotov.2013.2287758
10. J. Jhaveri, K. A. Nagamatsu, A. H. Berg, G. Man, G. Sahasrabudhe, S. Wagner, J. Schwartz, A. Kahn, and J. C. Sturm, "Double-heterojunction crystalline silicon solar cell with electron selective TiO2 cathode contact fabricated at 100 ^{o}C with open-circuit voltage of 640 mV," in 2015 IEEE 42nd Photovoltaic Specialist Conference, 2015. doi: 10.1109/PVSC.2015.7356054
11. K. A. Nagamatsu, S. Avasthi, G. Sahasrabudhe, G. Man, J. Jhaveri, A. H. Berg, J. Schwartz, A. Kahn, S. Wagner, and J. C. Sturm, "Titanium dioxide/silicon hole-blocking selective contact to enable double-heterojunction crystalline silicon-based solar cell," Applied Physics Letters, vol. 106, (2015). doi: 10.1063/1.4916540
12. S. Avasthi, K. A. Nagamatsu, J. Jhaveri, W. E. McClain, G. Man, A. Kahn, J. Schwartz, S. Wagner, and J. C. Sturm, "Double-heterojunction crystalline silicon solar cell fabricated at 250 oC with 12.9% efficiency," in 2014 IEEE 40th Photovoltaic Specialist Conference (PVSC), 2014, pp. 949-952. doi: 10.1109/PVSC.2015.7356054
13. J. A. Spechler, K. A. Nagamatsu, J. C. Sturm, and C. B. Arnold, "Improved efficiency of hybrid organic photovoltaics by pulsed laser sintering of silver nanowire network transparent electrode," ACS Applied Materials & Interfaces, vol. 7, pp. 10556-10562 (2015). doi: 10.1021/acsami.5b02203
14. G. Sahasrabudhe, S. M. Rupich, J. Jhaveri, A. H. Berg, K. A. Nagamatsu, G. Man, Y. J. Chabal, A. Kahn, S. Wagner, J. C. Sturm, and J. Schwartz, "Low-temperature synthesis of a TiO2/Si heterojunction," Journal of the American Chemical Society, vol. 137, pp. 14842-14845 (2015). doi: 10.1021/jacs.5b09750
15. A.H. Berg, G. S. Sahasrabudhe, R. A. Kerner, B. P. Rand, J. Schwartz, and J. C. Sturm, "Electron-blocking NiO/crystalline n-Si heterojunction formed by ALD at 175^{o}C," in 2016 74th Annual Device Research Conference (DRC), 2016, pp. 1-2. doi: 10.1109/DRC.2016.7548444
16. J. Jhaveri, A. H. Berg, S. Wagner, and J. C. Sturm, "Al/TiO2/p-Si heterojunction as an ideal minority carrier electron injector for silicon photovoltaics," in 2016 IEEE 43rd Photovoltaic Specialists Conference (PVSC), Portland, OR, 2016, pp. 2444-2447. doi: 10.1109/PVSC.2016.7750081

17. G. Man, J. Schwartz, J. C. Sturm, and A. Kahn, "Electronically Passivated Hole-Blocking Titanium Dioxide/Silicon Heterojunction for Hybrid Silicon Photovoltaics," Advanced Materials Interfaces, vol. 3, 1600026 (2016). doi: 10.1002/admi.201600026
18. A.H. Berg, K. A. Nagamatsu, and J. C. Sturm, "Extraction of Front- and Rear-Interface Recombination in Silicon Double-Heterojunction Solar Cells by Reverse Bias Transients," IEEE Transactions on Electron Devices, vol. 64, pp. 4518-4525 (2017). doi: 10.1109/TED.2017.2749525
19. A.H. Berg and J. C. Sturm, "Extracting interface recombination velocities from double-heterojunction solar cell reverse-recovery characteristics," in 2017 75th Annual Device Research Conference (DRC), 2017, pp. 1-2. doi: 10.1109/DRC.2017.7999506
20. Janam Jhaveri, Alexander H Berg, Sigurd Wagner, James C Sturm, “Measurement of TiO2/p-Si Selective Contact Performance using a Heterojunction Bipolar Transistor with a Selective Contact,” Proc. IEEE Photovoltaic Specialists Conf., Washington, DC, (June 25-30, 2017)

VII.C. Conference Presentations

1. S. Avasthi, W. McClain, J. Schwartz, and J. C. Sturm, "Hole-blocking TiO2/silicon heterojunction for silicon photovoltaics," in Device Research Conference (DRC), 2012 70th Annual, pp. 93-94, State College, PA, June, 2012. doi: 10.1109/DRC.2012.6256955
2. J. Jhaveri, S. Avasthi, G. Man, W. E. McClain, K. Nagamatsu, A. Kahn, J. Schwartz, and J. C. Sturm, "Hole-blocking crystalline-silicon/titanium-oxide heterojunction with very low interface recombination velocity," 2013 IEEE 39th Photovoltaic Specialists Conference (PVSC), Tampa, FL, June, 2013, pp. 3292-3296. doi: 10.1109/PVSC.2013.6745154
3. J. Jhaveri, S. Avasthi, K. A. Nagamatsu, and J. C. Sturm, "Wide bandgap HBT on crystalline silicon using electron-blocking PEDOT:PSS emitter," 2013 71st Annual Device Research Conference, pp. 77-78, South Bend, IN, June, 2013.
4. J. C. Sturm, S. Avasthi, K. Nagamatsu, J. Jhaveri, W. McClain, G. Man, A. Kahn, J. Schwartz, and S. Wagner, "Wide bandgap heterojunctions on crystalline silicon," in ULSI Process Integration 8 at the 224th Meeting of the Electrochem. Soc., San Francisco, CA, October, 2013; also Electrochem. Soc. Trans. vol. 58 (9), pp. 97-105, October, 2013. vol. 58, C. Claeys, et al., Eds., ed, 2013, pp. 97-105. doi: 10.1149/05809.0097ecst
5. J. A. Spechler, K. Nagamatsu, J. C. Sturm, and C. B. Arnold, "Integrated laser processed silver nanowire transparent electrodes with organic electronic devices," in 2013 Conference on Lasers and Electro-Optics, San Jose, CA, June 2013. doi: 10.1364/CLEO_SI.2013.CM1H.2
6. J. Jhaveri, S. Avasthi, K. Nagamatsu, and J. C. Sturm, "Stable low-recombination n-Si/TiO2 Hole-blocking interface and its effect on silicon heterojunction photovoltaics," in

2014 IEEE 40th Photovoltaic Specialist Conference (PVSC), pp. 1525-1528, Denver, CO, June, 2014, doi: 10.1109/PVSC.2014.6925206

7. S. Avasthi, K. A. Nagamatsu, J. Jhaveri, W. E. McClain, G. Man, A. Kahn, J. Schwartz, S. Wagner, and J. C. Sturm, "Double-heterojunction crystalline silicon solar cell fabricated at 250 ^{o}C with 12.9% efficiency," in 2014 IEEE 40th Photovoltaic Specialist Conference (PVSC), pp. 949-952, Denver, CO, June, 2014. doi: 10.1109/PVSC.2015.7356054
8. J. Jhaveri, G. Sahasrabudhe, G. Man, K. Nagamatsu, S. Wagner, A. Kahn, J. Schwartz, and J. C. Sturm, "Structure of low-temperature TiO2/Si interface and impact on surface recombination for low-cost Si-based PV," presented at the 45th IEEE Semiconductor Interface Specialists Conference, San Diego, CA, December, 2014.
9. K. A. Nagamatsu, S. Avasthi, J. Jhaveri, and J. C. Sturm, "A 12% efficient silicon/PEDOT:PSS heterojunction solar cell fabricated at < 100 ^{o}C," IEEE Journal of Photovoltaics, vol. 4, pp. 260-264 (2014). doi: 10.1109/jphotov.2013.2287758
10. J. Jhaveri, K. A. Nagamatsu, A. H. Berg, G. Man, G. Sahasrabudhe, S. Wagner, J. Schwartz, A. Kahn, and J. C. Sturm, "Double-heterojunction crystalline silicon solar cell with electron selective TiO_2 cathode contact fabricated at 100 ^{o}C with open-circuit voltage of 640 mV," in 2015 IEEE 42nd Photovoltaic Specialist Conference, New Orleans, LA, June, 2015. doi: 10.1109/PVSC.2015.7356054
11. A.H. Berg, G. S. Sahasrabudhe, R. A. Kerner, B. P. Rand, J. Schwartz, and J. C. Sturm, "Electron-blocking NiO/crystalline n-Si heterojunction formed by ALD at 175^{o}C," in 2016 74th Annual Device Research Conference (DRC), Newark, DE, June 2016. doi: 10.1109/DRC.2016.7548444
12. J. Jhaveri, A. H. Berg, S. Wagner, and J. C. Sturm, "Al/TiO2/p-Si heterojunction as an ideal minority carrier electron injector for silicon photovoltaics," in 2016 IEEE 43rd Photovoltaic Specialists Conference (PVSC), Portland, OR, 2016, pp. 2444-2447. doi: 10.1109/PVSC.2016.7750081
13. Plenary Talk: James C. Sturm, “Widegap Heterojunctions on Silicon,” Joint Int. Symp. on Control of Semicond. Interfaces-VII / International Silicon-Germanium (ISTDM) Technology & Device Meeting, Nagoya, Japan, June, 2016.
14. A.H. Berg and J. C. Sturm, "Extracting interface recombination velocities from double-heterojunction solar cell reverse-recovery characteristics," in 2017 75th Annual Device Research Conference (DRC), South Bend, IN, June, 2017, pp. 1-2. doi: 10.1109/DRC.2017.7999506
15. Janam Jhaveri, Alexander H Berg, Sigurd Wagner, James C Sturm, “Measurement of TiO2/p-Si Selective Contact Performance using a Heterojunction Bipolar Transistor with a Selective Contact,” IEEE Photovoltaic Specialists Conf., Washington, DC, June 25-30, 2017.

VII.D. Awards and Honors

Best Poster Award: Janam Jhaveri received Best Poster Award at the 2015 IEEE Photovoltaic Specialists Conference for "Double-Heterojunction Crystalline Silicon Solar Cell with Electron-Selective TiO_2 Cathode Contact Fabricated at 100 ^oC with Open Circuit Voltage of 640mV".

Plenary Talk: James C. Sturm, "Widegap Heterojunctions on Silicon," Joint Int. Symp. on Control of Semicond. Interfaces-VII / International Silicon-Germanium (ISTDM) Technology & Device Meeting, Nagoya, Japan, June, 2016

2016 Siebel National Energy Scholar: Graduate student Janam Jhaveri is the sole Princeton awardee, http://www.siebelscholars.com/